AGU100 ADVANCING EARTH AND SPACE SCIENCE

Tectonics

RESEARCH ARTICLE
10.1029/2018TC004994

This article is a companion to Jackson et al. (2018) https://doi.org/10.1029/2018TC004995.

Key Points:
- Nonmarine fill of the Mula basin in the southern Yidun terrane consists of Cenozoic alluvial strata
- Provenance analyses suggest that sediment was locally sourced from Triassic Yidun terrane rock
- The Mula basin developed in a contractional tectonic setting in response to the India-Asia collision

Supporting Information:
- Table S1
- Data Set S1

Correspondence to:
W. T. Jackson Jr.,
wjackson@southalabama.edu

Citation:
Jackson, W. T., Jr., Robinson, D. M., Weislogel, A. L., Jian, X., & McKay, M. P. (2018). Cenozoic development of the nonmarine Mula basin in the Southern Yidun terrane: Deposition and deformation in the eastern Tibetan Plateau associated with the India-Asia collision. *Tectonics*, *37*. https://doi.org/10.1029/2018TC004994

Received 22 JAN 2018
Accepted 30 MAY 2018
Accepted article online 7 JUN 2018

Cenozoic Development of the Nonmarine Mula Basin in the Southern Yidun Terrane: Deposition and Deformation in the Eastern Tibetan Plateau Associated with the India-Asia Collision

W. T. Jackson Jr.[1,2], D. M. Robinson[2], A. L. Weislogel[3], X. Jian[4], and M. P. McKay[5]

[1]Department of Earth Sciences, University of South Alabama, Mobile, AL, USA, [2]Department of Geological Sciences and Center for Sedimentary Basin Studies, The University of Alabama, Tuscaloosa, AL, USA, [3]Department of Geography and Geology, West Virginia University, Morgantown, WV, USA, [4]College of Ocean and Earth Sciences, Xiamen University, Xiamen, China, [5]Department of Geography, Geology, and Planning, Missouri State University, Springfield, MO, USA

Abstract To advance tectonic models of plateau growth in response to the India-Asia collision, parameters such as the timing, mechanism (s), and extent of Cenozoic deposition and deformation throughout the eastern Tibetan Plateau need to be determined. To better understand these parameters, we examine the Mula basin, located in the southern Yidun terrane, using field data, detrital zircon geochronology, εHf zircon isotopic values, and thin section petrology. The Mula basin is a NW-SE elongate (~28 km long and 5–8 km wide) exposure of nonmarine strata ~1,000 m thick, deposited in alluvial environments. The basin is bound to the northeast by a thrust fault (327, 34°NE) that places Triassic Daocheng Pluton and Triassic Yidun Group rocks on top of the nonmarine strata. The western boundary is defined by an unconformable contact between the overlying nonmarine strata and Triassic Daocheng Pluton and Yidun Group rock. An intrabasin thrust fault, parallel to the basin-bounding fault, places older nonmarine strata on top of younger nonmarine strata, illustrating postdepositional deformation. Provenance results indicate that sediment influx originated primarily from localized drainage catchments and lacked major, well-organized throughgoing systems. A maximum depositional age of 45.5 ± 0.5 Ma, based on the weighted mean average of the youngest detrital zircon population (s), demonstrates an Eocene or younger age for strata. We interpret the Mula basin to have developed in a contractional deformational regime driven by a far-field, upper-crustal response associated with the transition from an Andean style margin to a continent-continent collisional margin as India impinged upon Eurasia.

1. Introduction

The present-day Tibetan Plateau developed as a result of the India-Asia collision, which initiated at ~55–60 Ma (DeCelles et al., 2014; Hu et al., 2016; Leech et al., 2005; Najman et al., 2010; Wang et al., 2011). Because ongoing collisional processes between the Indian and Asian lithosphere can be observed and measured, and because the plateau is the largest and highest on Earth, researchers use the Tibetan Plateau to generate ideas regarding tectonic processes driving plateau development. Models aimed at describing the development of the Tibetan Plateau have invoked mechanisms such as underthrusting of the Indian lithosphere (DeCelles et al., 2002; Nabelek et al., 2009; Owens & Zandt, 1997; Powell, 1986; Zhao & Morgan, 1987), rigid block translation (Meade, 2007; Tapponnier et al., 1982, 2001; Thatcher, 2007), distributed continuum deformation (Dayem et al., 2009; England & Houseman, 1986, 1989; England & McKenzie, 1982; England & Searle, 1986) with associated convective removal of mantle lithosphere (Molnar et al., 1993), and middle to lower crustal flow (Clark & Royden, 2000; Royden et al., 1997; Schoenbohm et al., 2006). To provide initial crustal parameters that can be used to evaluate these models, spatial and temporal resolutions of deposition and deformation associated with the India-Asia collision must be determined. Therefore, stratigraphic ages, sedimentological descriptions, and structural relationships for Cenozoic strata throughout the Tibetan Plateau (Figure 1) are essential for accurately describing the progression, amount, and mechanism(s) of deformation associated with the India-Asia collision (DeCelles, Kapp, et al., 2007; Horton et al., 2002, 2004; Yin & Harrison, 2000).

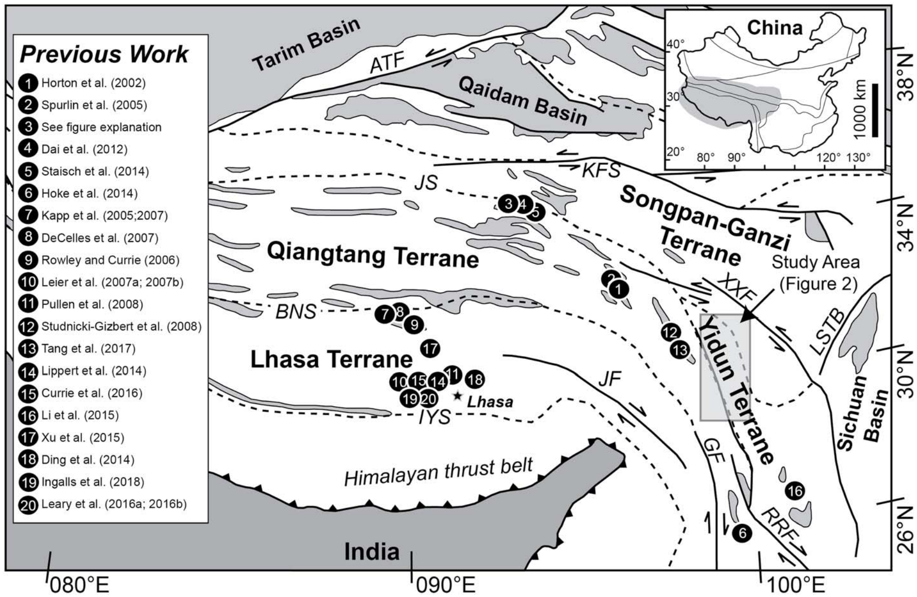

Figure 1. Distribution of Cenozoic nonmarine strata, faults, and suture zones throughout the Tibetan Plateau. The shaded area indicates the study area and location of the Mula basin (boundary for Figure 2a). Map adapted from Yin and Harrison (2000), Horton et al. (2002), and Spurlin et al. (2005). (top left insert) Outline of China with >3.5-km topographic expression of the Tibetan Plateau (gray shading) and major suture zones delineated. (bottom left insert) Previous studies conducted on nonmarine strata throughout the Tibetan Plateau summarized herein. Number 3: Yin et al. (1988), Zhang and Zheng (1994), Liu and Wang (2001), Liu et al. (2001), and Liu et al. (2003). ATF: Altyn Tagh fault; BNS: Bangong-Nujiang suture; JS: Jinsha suture; KFS: Kunlun fault system; LSTB: Longmen Shan thrust belt; RRF: Red River fault.

Cenozoic nonmarine strata in the southern Tibetan Plateau's Lhasa terrane provide insights into the timing of India-Asia collision (Ding et al., 2005; Orme et al., 2015), the latitudinal migration of the southern margin of Eurasia (Lippert et al., 2014), the pervasive tectonic stress regime (Leary, DeCelles, et al., 2016; Leary, Orme, et al., 2016), reconstructions of paleoelevations (Currie et al., 2016; DeCelles, Kapp, et al., 2007; Ding et al., 2014; Ingalls et al., 2018; Rowley & Currie, 2006), and paleo-drainage reconstructions (Leier, DeCelles, et al., 2007; Carrapa et al., 2017). Cenozoic nonmarine strata in the northern Tibetan Plateau record the timing of initial, far-field deformation associated with the India-Asia collision (e.g., Clark et al., 2010), while nonmarine strata in the southeastern part of the plateau record the clockwise rotation and crustal block extrusion of the Lanping-Simao terrane (Schoenbohm et al., 2005, 2006).

In contrast to other regions of the Tibetan Plateau, nonmarine successions in the eastern Tibetan Plateau remain understudied. The Yidun terrane, positioned between the eastern Himalayan syntaxis and the Xianshuihe fault system, hosts numerous nonmarine basins (Burchfiel & Chen, 2012; Wang et al., 2009; Wang & Burchfiel, 2000). Because of the Yidun terrane's position, investigating these nonmarine basins presents an opportunity to gain insight into the Cenozoic tectonic evolution of the eastern Tibetan Plateau.

The purpose of this study is to document sedimentological and structural data from the nonmarine Mula basin, located in the southern Yidun terrane (Figure 2). Determining the tectonic development of the Mula basin and incorporating our findings into a regional perspective will allow for an enhanced understanding of the spatial and temporal evolution of nonmarine deposition and deformation throughout the eastern Tibetan Plateau. We present detrital U-Pb zircon geochronology and εHf isotope values, as well as traditional provenance analyses and field measurements to address the tectonic setting, stratigraphic age, and sedimentary provenance of the Mula basin fill.

2. Geologic Setting

The eastern Tibetan Plateau consists of a mosaic of terranes that include the Lhasa, Qiangtang, Yidun, and Songpan-Ganzi, all separated by Paleo- and Meso-Tethys ocean sutures. These terranes contain records of Paleozoic-Mesozoic rifting and migration from Gondwana, followed by amalgamation to the southern

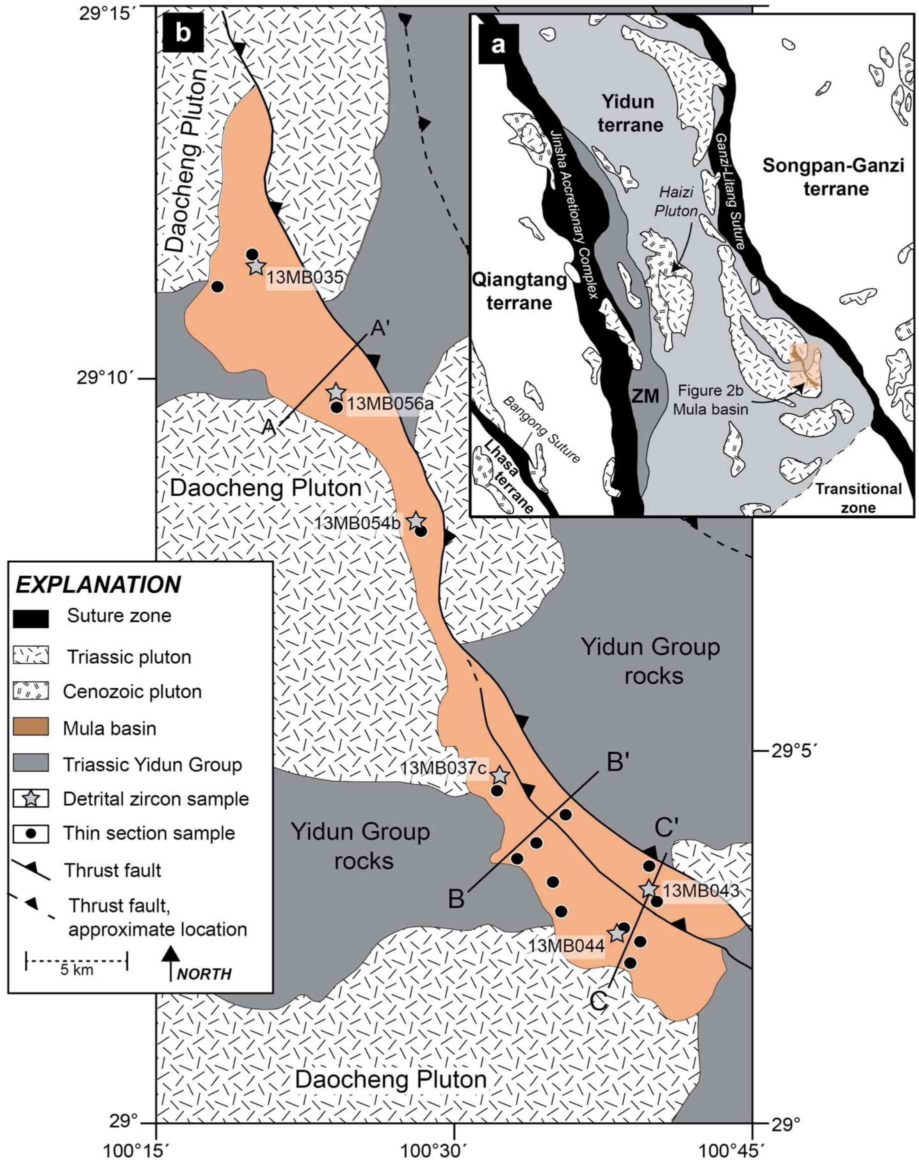

Figure 2. (a) Regional map of the eastern Tibetan Plateau adapted from Burchfiel and Chen (2012) and Wang et al. (2013). (b) Geologic map of the Mula basin region with locations of detrital zircon and petrology samples.

margin of Eurasia, while the intervening suture zones contain mélange and ophiolite rock that record the closure of ocean basins (Burchfiel & Chen, 2012; Dewey et al., 1988; Yin & Harrison, 2000). The Zhongza Massif, which now forms the western part of the Yidun terrane, rifted from either the western margin of the Yangtze block (Wang et al., 1999; Zhang et al., 1998) or the southern Kunlun terrane (Ding et al., 2013; Pullen, Kapp, Gehrels, Vervoort, et al., 2008) during Early Triassic time. In the wake of the Zhongza Massif migration, an eastern branch of the Paleo-Tethys Ocean was formed, which contributed space for widespread deposition of the Songpan-Ganzi and Yidun terrane turbidite complexes during Middle-Late Triassic time (Roger et al., 2010; Zhang et al., 1998). The Zhongza Massif collided with the Qiangtang terrane during Middle Triassic time, presently marked by the Jinsha Accretionary Complex (Reid, et al., 2005). In Late Triassic time, subduction along the eastern Yidun terrane was initiated, marked presently by the Ganzi-Litang suture and Yidun Arc Late Triassic plutonic field (Hou, 1993; Hou et al., 1993; Peng et al., 2014). In Late Jurassic-Middle Cretaceous time, the Lhasa terrane collided with the southern margin of the Qiangtang terrane (Kapp et al., 2005). In Late Cretaceous time northward subduction of the Neo-Tethys beneath the southern margin of the Lhasa terrane initiated, resulting in the development of the Gangdese magmatic belt (Ding et al., 2005; Van der Voo et al., 1999; Zhang et al., 2010). While much still remains to be understood pertaining to these Mesozoic collisional events, they ultimately resulted in an Andean-like margin along the southern margin of Eurasia during Late Cretaceous-Paleogene time, forming a fore arc, continental magmatic arc, and retroarc foreland basin (Kapp et al., 2003, 2007; Leier, DeCelles, et al., 2007; Murphy et al., 1997; Pullen, Kapp, Gehrels, DeCelles, et al., 2008), as well as the development of a concomitant plateau (C. Wang et al., 2008; Zhang et al., 2012).

Following Mesozoic terrane collisions, India rifted from Gondwana, migrated northward as the Neo-Tethys Ocean subducted, and collided with southern Eurasia in early Cenozoic time (Hu et al., 2016; Royden et al., 2008, references therein). Paleogene deformation in response to this initial collision is marked by compressional structures and nonmarine deposition throughout the plateau (Yin & Harrison, 2000). In the eastern Tibetan Plateau, during early Cenozoic time, contractional upper-crustal shortening persisted in conjunction with the initiation of southeastward extrusion of crustal blocks in response to continental collision (Burchfiel et al., 1995; Tapponnier et al., 1982, 2001; Wang & Burchfiel, 1997). During late Miocene time strike-slip deformation became the prominent stress regime and further propagated extrusion of crustal material to the southeast (Leloup et al., 1995; Schoenbohm et al., 2005, 2006). Paleomagnetic studies on Late Cretaceous through Miocene rocks in the southeastern Tibetan Plateau indicate a significant clockwise rotation of crustal material since Late Cretaceous time (Haihong et al., 1995; Holt et al., 1991; Huang & Opdyke, 1993).

3. Previous Work

Throughout the Tibetan Plateau, nonmarine Cenozoic strata record upper-crustal deposition and deformation associated with plateau growth (Yin & Harrison, 2000). These strata tend to be in basins that are elongate in shape, located in the footwalls of thrust faults, and spatially associated with Mesozoic sutures (e.g., Spurlin et al., 2005; Studnicki-Gizbert et al., 2008). While precise dating of these basins is difficult (Horton et al., 2004), nonmarine strata throughout the plateau have been assigned Paleogene ages based on fossil assemblages, geochronology, and palynological data (BGMRSP, 1991; Dai et al., 2012; Liu et al., 2001; Rowley & Currie, 2006; Staisch et al., 2014). Over the past two decades, reconstructions of paleoelevation from nonmarine strata provide the stimulus for debates on the timing of established high-topography and tectonic evolution of the Tibetan Plateau (Currie et al., 2016; DeCelles, Carrapa, et al., 2007; Ding et al., 2014; Ingalls et al., 2018; Rowley & Currie, 2006; Xu et al., 2015). The geographic locations of the nonmarine strata discussed below are in Figure 1.

3.1. Southern Tibetan Plateau

In the southern Lhasa terrane, the Late Cretaceous Takena Formation consists of nonmarine strata developed in a retroarc foreland basin with sediment derived primarily from the Gangdese volcanic arc (Leier, DeCelles, et al., 2007). The tectonic setting and development of the Takena Formation suggest that the southern margin of the Lhasa terrane was characterized by thickened crust and was likely at high elevations immediately prior to the India-Asia collision (England & Searle, 1986; Leier, DeCelles, et al., 2007). Detrital zircon geochronology results from the Takena Formation reveal age populations at 100–160 Ma, 500 Ma, 600 Ma, 1,000 Ma, and 1,400 Ma indicative of a typical Lhasa terrane signature (Leier, Kapp, et al., 2007). Lippert et al. (2014) summarize paleomagnetic data in the Lhasa terrane and show that the southern margin of Eurasia (Lhasa terrane) remained stable in latitude throughout Cretaceous and Early Paleogene time and subsequently has moved ~8° of latitude since ~50 Ma.

3.2. Central Tibetan Plateau

Kapp et al. (2005) document Middle Cretaceous nonmarine strata unconformably overlying Jurassic suture zone rock in the Qiangtang terrane anticlinorium. Paleogene deformation in the Qiangtang terrane is characterized by north-dipping thrust faults that cut Eocene-Oligocene redbeds and volcanic rocks in the footwall. Two footwall volcanic tuff layers were dated at 64 and 43 Ma (Kapp et al., 2005). Cretaceous deformation and denudation are attributed to northward underthrusting of the Lhasa terrane beneath the Qiangtang terrane along the Bangong-Nujiang suture.

Kapp et al. (2007) and DeCelles, Kapp, et al. (2007) document nonmarine deposition and deformation in the Nima region along the Bangong-Nujiang suture. Dating of a cross-cutting intrusion establishes a 118-Ma age for the oldest nonmarine strata, which overlie deep marine strata with a maximum depositional age of

125 Ma, therefore bracketing the transition from deep marine to subaerial deposition and closure timing of the Bangong-Nujiang suture to between 118 and 125 Ma (Kapp et al., 2007). Cretaceous-Paleogene sedimentation was coeval with thrust-faulting, which resulted from northward low-angle subduction of the Neo-Tethys oceanic lithosphere and Lhasa-Qiangtang terrane collision (DeCelles, Kapp, et al., 2007). Oxygen-isotope analysis of carbonate nodules indicates regional paleoelevations of >4.6 km during late Oligocene time (DeCelles, Kapp, et al., 2007). Rowley and Currie (2006) also document paleoelevations of >4 km in Eocene time for the Lunpola basin in the Lhasa terrane based on oxygen isotopes.

Horton et al. (2002) document nonmarine sedimentation synchronous with Paleocene-Eocene NE-SW shortening in the Nangqian-Niuguoda-Xialaxiu-Shanglaxiu basins, located in the Qiangtang terrane. Spurlin et al. (2005) establish an Eocene age for basins in the Yushu-Nangqian region and quantify minimum NE-SW shortening at 61 km. Spurlin et al. (2005) show that igneous intrusive rocks are subduction related, suggesting that crustal thickening during Eocene time resulted from continent subduction.

3.3. North-Central Tibetan Plateau

The predominantly nonmarine Hoh Xil basin is located in the northern part of the Qiangtang terrane (Liu et al., 2001; Liu & Wang, 2001). Based on fossil assemblages and magnetostratigraphy, the stratigraphically lowest Fenghuoshan Group is Paleogene (Yin et al., 1988) and Cretaceous (Liu et al., 2003; Zhang & Zheng, 1994) in age. The stratigraphic highest Wudaoling Group is early Miocene (23–16 Ma) in age based on fossil assemblages (Zhang & Zheng, 1994). Staisch et al. (2014) establish an age of Late Cretaceous-Eocene (85–51 Ma) for nonmarine strata based on detrital zircon geochronology. Dai et al. (2012) establish a detrital zircon maximum depositional age for the nonmarine strata of 121 Ma. Sedimentary provenance analysis from petrology and detrital zircon geochronology suggests that strata were sourced locally from the Qiangtang terrane (Dai et al., 2012; Liu et al., 2001; Staisch et al., 2014).

3.4. Eastern Tibetan Plateau

Studnicki-Gizbert et al. (2008) document Paleogene nonmarine deposition and associated compressional deformation in the Gonjo basin, resulting from the early stages of the India-Asia collision. Studnicki-Gizbert et al. (2008) illustrate a local provenance for Gonjo sedimentary rocks and document coaxial trends for Mesozoic and Cenozoic structures, illustrating the difficulty in distinguishing between the multiple phases of deformation. Tang et al. (2017) establish deposition of Gonjo basin strata prior to 43.2 Ma based on U-Pb dating of volcanic rocks and indicate the basin attained elevations of 2.1–2.5 km in early Eocene time from oxygen and carbon stable isotope results.

3.5. Southeastern Tibetan Plateau

Li et al. (2015) use oxygen isotope data from three Cenozoic sedimentary basins in the southeastern Tibetan Plateau, to suggest that elevations of ~2.6 km may have persisted since middle Eocene time (~40 Ma). Hoke et al. (2014) utilize carbonate isotope data to evaluate the paleoaltimetry of the southeastern margin of the Tibetan Plateau, in which they show that the southern Tibetan Plateau established its modern-day elevations as early as Eocene time. Both of these studies postulate that crustal shortening played a dominant role in thickening the crust and associated elevation gain, whereas middle to lower-crustal flow did not affect the region until Miocene time.

3.6. Northeastern Tibetan Plateau

Horton et al. (2004) show nonmarine deposition and deformation in the Xining-Minhe and Dangchang basins. Basin deposition and deformation is characterized by Late Jurassic-Early Cretaceous extension and Cretaceous-Paleogene postrift thermal subsidence, followed by Eocene (40–30 Ma) shortening related to the India-Asia collision. Craddock et al. (2012) document nonmarine deposition associated with SE verging thrust faults and establish an Early Cretaceous age.

4. Methods

4.1. Field Procedures

The Mula basin was studied over three field seasons in 2013 and 2014. Rock samples were collected for detrital zircon geochronology and thin section petrology. Sampling distribution and density were controlled primarily by rock type and accessibility. Field data were collected to document the sedimentological and structural relationships present. Detailed rock descriptions, field measurements, and sample locations are in Table S1.

4.2. Detrital Zircon Geochronology

Six samples from the Mula basin were analyzed for detrital zircon geochronology. One to 4 kg of sample were collected from sandstone and granule conglomerate. Zircon grains were separated using heavy mineral separation methods at the University of Alabama. Unknown Mula zircon grains, along with standard Sri Lanka (Gehrels et al., 2006; Kroner et al., 1987) and R33 (Black et al., 2004) zircon fragments, were mounted (2.45-cm epoxy), abraded, polished, and imaged (back scatter electron) at the University of Arizona LaserChron Center following procedures described in Gehrels et al. (2008) and Gehrels (2014). Ages were collected with a Nu Plasma multicollector LA-ICP-MS (sample 13MB037c) and an Element 2 single collector LA-ICP-MS (samples 13MB043, 13MB044, 13MB035, 13MB054b, and 13MB056a). Zircon grains were ablated with 25–30 μm diameter laser. Zircon data reduction (background, Hg, and fractionation corrections) were calculated in the excel software program Agecalc (Gehrels et al., 2008). Isotopic age uncertainties were additionally evaluated based on the amount of ^{204}Pb, concordance, and concentration of U and Th (ppm). Grains >900 Ma (based on ^{206}Pb/^{207}Pb ages) were plotted in concordia space and evaluated based on 25% discordant or 5% reverse-discordant criteria. Grains <900 Ma (based on ^{206}Pb/^{238}U ages) were plotted in concordia space for evaluation. Therefore, the variability in number of zircon analyses per sample is a result of zircon yield, time and cost, and frequency of discordant analysis. Zircon data are in figures produced in Isoplot (Ludwig, 2012) and DensityPlotter (Vermeesch, 2012). Full U-Pb analytical data are in Table S2.

As no diagnostic fossils, dateable volcanic ash layers, or cross-cutting intrusive bodies were identified, we utilized detrital zircon geochronology to calculate maximum deposition ages (MDAs). MDAs are calculated based on the youngest analyzed zircon grain(s), especially for strata that otherwise do not yield any information pertaining to their age (i.e., Barbeau et al., 2009; DeCelles, Carrapa, et al., 2007; Dickinson & Gehrels, 2009; Fildani et al., 2003; Surpless et al., 2006). However, many geologic factors such as a lull in deposition, isolation of source material, and field/lab contamination can cause the youngest zircon age(s) to be tens to hundreds of million years older than the true depositional age (Nelson, 2001; Sircombe, 1999). In addition, only using the youngest detrital zircon grain to determine the MDA may produce an age younger than the true depositional age (Dehler et al., 2010; Dickinson & Gehrels, 2003, 2009). Therefore, a more reliable approach is to calculate the weighted mean average of the youngest zircon population with an n value of ≥3 (Dickinson & Gehrels, 2009; Vermeesch, 2004).

4.3. Detrital Zircon εHf Isotopes

Sixty-two detrital zircon grains were analyzed for εHf-isotopic values by LA-ICP-MS at the University of Arizona LaserChron Center following methods described by Gehrels and Pecha (2014). Data were collected using a Nu Plasma HR ICP-MS, coupled to a New Wave 193-nm ArF laser ablation system from existing pits from previously analyzed detrital U-Pb zircon grains to best ensure that the initial εHf isotope data were determined from the same domain as the U-Pb age. An average of 10 analyses were collected from each sample, with the goal to represent each of the prominent age populations identified from U-Pb geochronology analyses. Full εHf data are in Table S3.

4.4. Petrology

Fifteen thin sections from Mula basin samples were prepared for petrographic analysis. Mineral staining was included for assistance in potassium feldspar and calcic plagioclase identification. Minerals documented include monocrystalline quartz, polycrystalline quartz, plagioclase feldspar, potassium feldspar, volcanic/meta-volcanic lithic fragments, sedimentary/meta-sedimentary lithic fragments, and matrix. Four hundred framework grains were counted for each sample following the Ganzi-Dickinson method to minimize grain-size effects (Dickinson, 1970; Ingersoll et al., 1984). Results were plotted in the following ternary spaces: (1) quartz total, feldspar, lithics; (2) monocrystalline quartz, feldspar, lithic total; (3) monocrystalline quartz, plagioclase, potassium feldspar; and (4) polycrystalline quartz, volcanic lithics, sedimentary lithics to asses associated tectonic settings (Dickinson, 1985; Dickinson & Suczek, 1979; Ingersoll, 1978), using an excel-based method by Zahid and Barbeau Jr. (2011). Full petrology data are in Table S4.

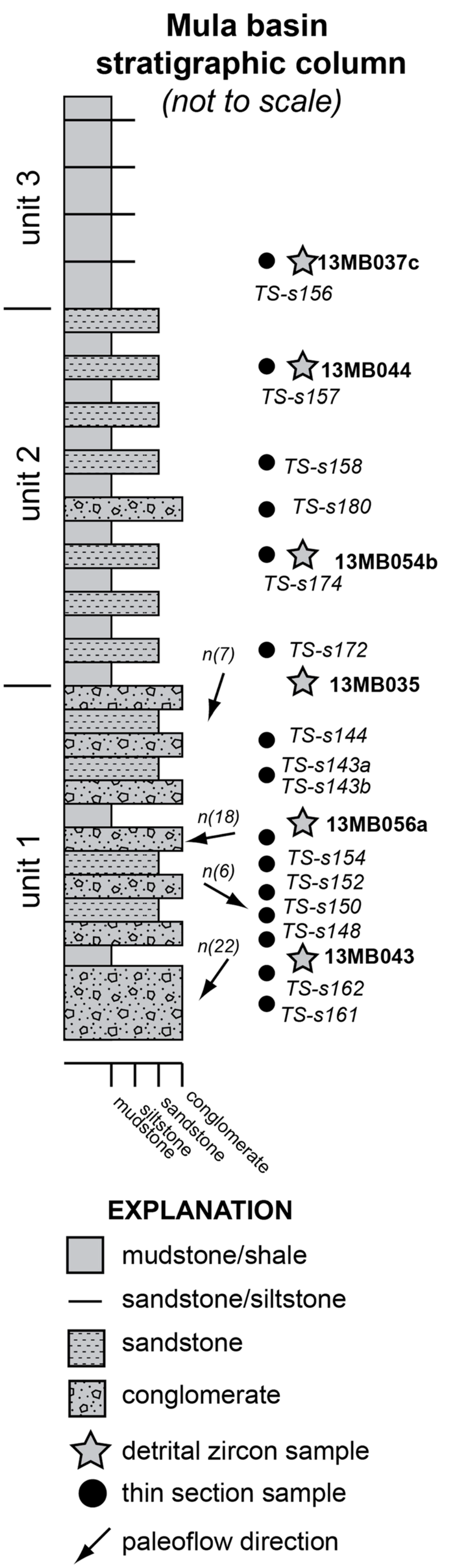

Figure 3. Stratigraphic column for the Mula basin illustrating rock type, location of detrital zircon and thin section petrology samples, and measured paleoflow directions.

5. Results

5.1. Mula Basin Stratigraphy

The Mula basin contains ~1,000 m of oxidized, red to purple nonmarine strata in three units (Figure 3). The stratigraphic lowest is unit 1, which consists of an ~5–20 m thick basal conglomerate overlain by ~200–250 m of interbedded conglomerate, sandstone, and mudstone. Unit 1 basal conglomerate clasts are pebble to cobble in size, predominantly matrix-supported, with <0.5 m thick clast-supported intrabeds, unconformably overlying the Triassic Yidun Group and Triassic Daocheng Pluton. Clasts are subangular to subrounded and consist of shale, granite, quartz, sandstone, and chert (Figure 4a). Bedding is tabular with no evidence of channel bases. Clast imbrication (n = 53) in clast-supported conglomerate intrabeds indicate paleoflow directions to the southwest, west, and southeast. Above the basal conglomerate is an interbedded sequence of conglomerate, sandstone, and mudstone (Figures 4b–4d). Conglomerate beds are ~0.5–3 m thick, clast-supported, with subrounded granule-sized clasts. Sandstone beds are ~0.5–3 m thick, fine- to medium-grained, subrounded, predominately feldspathic arenites, although lithic arenites are present. Overall, unit 1 fines upward.

Stratigraphically above unit 1, unit 2 consists of an ~500–600 m thick sequence of interbedded sandstone and mudstone, with occasional conglomerate beds (Figure 4e). Sandstone beds are ~0.5–3 m thick, fine- to medium grained, subrounded, predominately feldspathic arenites, although lithic arenites are present. Mudstone beds throughout unit 2 are massive and range in thickness from tens of cm to hundreds of m. Overall, unit 2 fines upward.

Stratigraphically above unit 2, unit 3 consists of a 200–300 m thick sequence of mudstone and shale, with thin (<2 m) sandstone and siltstone beds. Mudstone beds throughout unit 3 are massive with variable bedding thickness. Sandstone and siltstone intrabeds are well-sorted, subrounded to rounded, feldspathic arenites and lithic arenites. The uppermost part of unit 3 is dominated by mudstone and shale that displays fissile bedding and green, purple, and red coloring. Unit 3 does not show a stratigraphic textural pattern.

5.2. Detrital Zircon Geochronology

Cumulative detrital zircon geochronology results (n = 1,502) from the six Mula basin samples illustrate one primary age population at 200–250 Ma, along with minor populations at 40–60 Ma, 250–450 Ma, 700–850 Ma, ~1,800–1,900 Ma, and ~2,500 Ma (Figure 5). The 200–250 Ma population represents 45.3% of calculated ages. The second largest population is the ~1,800 Ma peak, consisting of 14.9%. The youngest population is 40–60 Ma, representing 5.1% of total analyzed grains. The other 3 populations present at 250–450 Ma, 700–850 Ma, and ~2,500 Ma constitute 8.7%, 6%, and 5.7% of the cumulative distribution, respectively.

Sample 13MB037c is the highest stratigraphic sample and yields 90 ages with evidence of all major age populations present in the cumulative data set, with peaks at 40–50 Ma, 200–250 Ma, 250–350 Ma, 400–500 Ma, ~1,200 Ma, ~1,800 Ma, ~2,200 Ma, and ~2,500 Ma (Figure 5a). Eight zircon grains from 13MB037c have ages between 40 and 50 Ma, with the youngest grain at 42 Ma. 13MB044 is located stratigraphically below sample 13MB037c and yields 313 ages with evident age populations at 40–50 Ma, 200–250 Ma, 250–350 Ma, ~400 Ma, ~1,800 Ma, and ~2,500 Ma

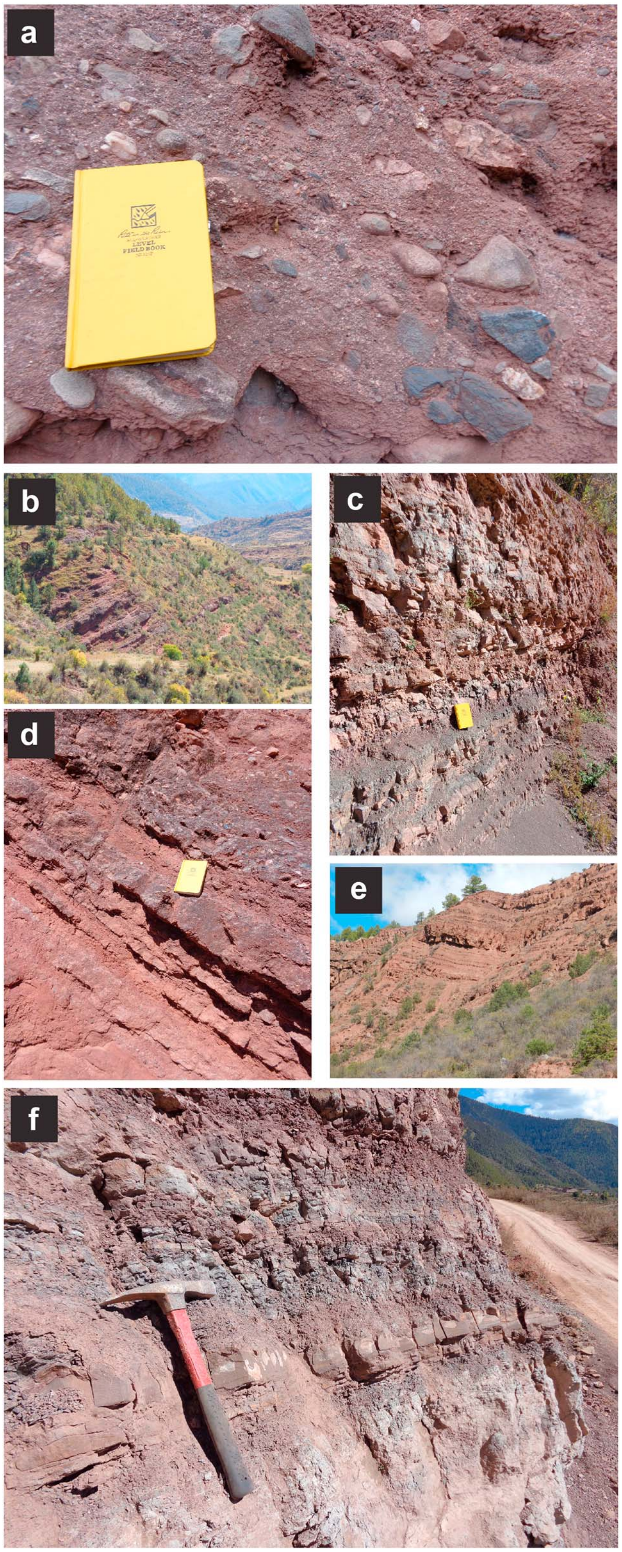

Figure 4. Field photographs from the Mula basin illustrating examples of units 1–3 stratigraphic intervals. (a) Unit 1 matrix-supported conglomerate with various locally derived clasts. (b) Unit 1 interbedded conglomerate and mudstone/siltstone. (c) Unit 1 interbedded conglomerate, sandstone, and mudstone. (d) Unit 2 interbedded sandstone, mudstone, and conglomerate. (e) Unit 2 interbedded sandstone and mudstone. (f) Unit 3 interbedded shale and siltstone.

(Figure 5b). Thirty-six zircon grains from 13MB044 have ages between 40 and 50 Ma, with the youngest grain at 43 Ma. 13MB054b is located stratigraphically below sample 13MB044 and yields 312 ages with evident age populations at 40–50 Ma, 200–250 Ma, 300–400 Ma, ~800 Ma, ~1,800 Ma, and ~2,500 Ma (Figure 5c). Ten zircon grains from 13MB054b have ages between 40 and 50 Ma, with the youngest grain at 44 Ma. 13MB043 is located stratigraphically below sample 13MB054b and yields 207 ages with evident age populations at 200–250, ~300–400 Ma, ~800 Ma, ~1,800 Ma, and ~2,500 Ma (Figure 5d). Two zircon grains from 13MB043 have ages between 40 and 50 Ma, with the youngest grain at 44 Ma. 13MB035 is located stratigraphically below sample 13MB043 and yields 292 ages with one evident population at 200–250 Ma (Figure 5e). Two zircon grains from 13MB035 have ages between 40 and 50 Ma, with the youngest grain at 42 Ma. 13MB056a is the stratigraphic lowest sample and yields 288 ages with only one evident population at 250–200 Ma (Figure 5f). Three zircon grains from sample 13MB056a have ages between 40 and 50 Ma, with the youngest grain at 44 Ma.

5.3. Detrital Zircon εHf Analysis

εHf isotope analytical results (Figure 6) show that 66% of analyzed zircons have negative εHf values (41 of 62 grains). Eocene-aged grains have εHf values of +4 to −4. Triassic-aged grains have εHf values clustered between −5 and −9. Devonian-Cambrian grains range from εHf +8 to −27. Neoproterozoic age grains have εHf values from +7 to −2. Paleoproterozoic age grains cluster between εHf 2 and −4. Paleoproterozoic-Archean age grains have εHf values of +5 to −5.

5.4. Petrology

Framework-grain modal composition in 13 of 15 samples plot in the recycled orogenic field for the quartz total, feldspar, lithics provenance discrimination ternary diagram, while 2 of 15 plot in the dissected arc field (Figure 7a). The 15 samples plot in the transitional recycled, recycled orogenic, mixed fields for the monocrystalline quartz, feldspar, lithic total ternary diagram (Figure 7b). All 15 samples plot in the recycled orogeny field for the monocrystalline quartz, plagioclase, potassium feldspar ternary diagram (Figure 7c). Of 15 samples, 13 plot in the collision suture and fold-thrust belt source field for the polycrystalline quartz, volcanic lithics, sedimentary lithics ternary diagram (Figure 7d).

5.5. Structure

The Mula basin is elongate to the NW-SE with beds oriented ~330, 24–38°E. To the southwest, the Mula basin is bound by unconformable contacts with the Triassic Daocheng Pluton and Triassic Yidun Group turbidite rock. To the northeast, the Mula basin is bound by a reverse fault oriented ~327, 34°NE that places Triassic Yidun Group turbidite rock on top of nonmarine basin strata (Figures 8a–8c). Another reverse fault mapped in the southern part of the basin is oriented parallel to the basin-bounding fault and places unit 2 strata in the hanging wall on top of unit 3 strata in the footwall (Figures 8b and 8c). The intrabasin fault decreases in offset toward the northwest, where it branches into the basin-bounding fault. No growth strata are present in the Mula basin.

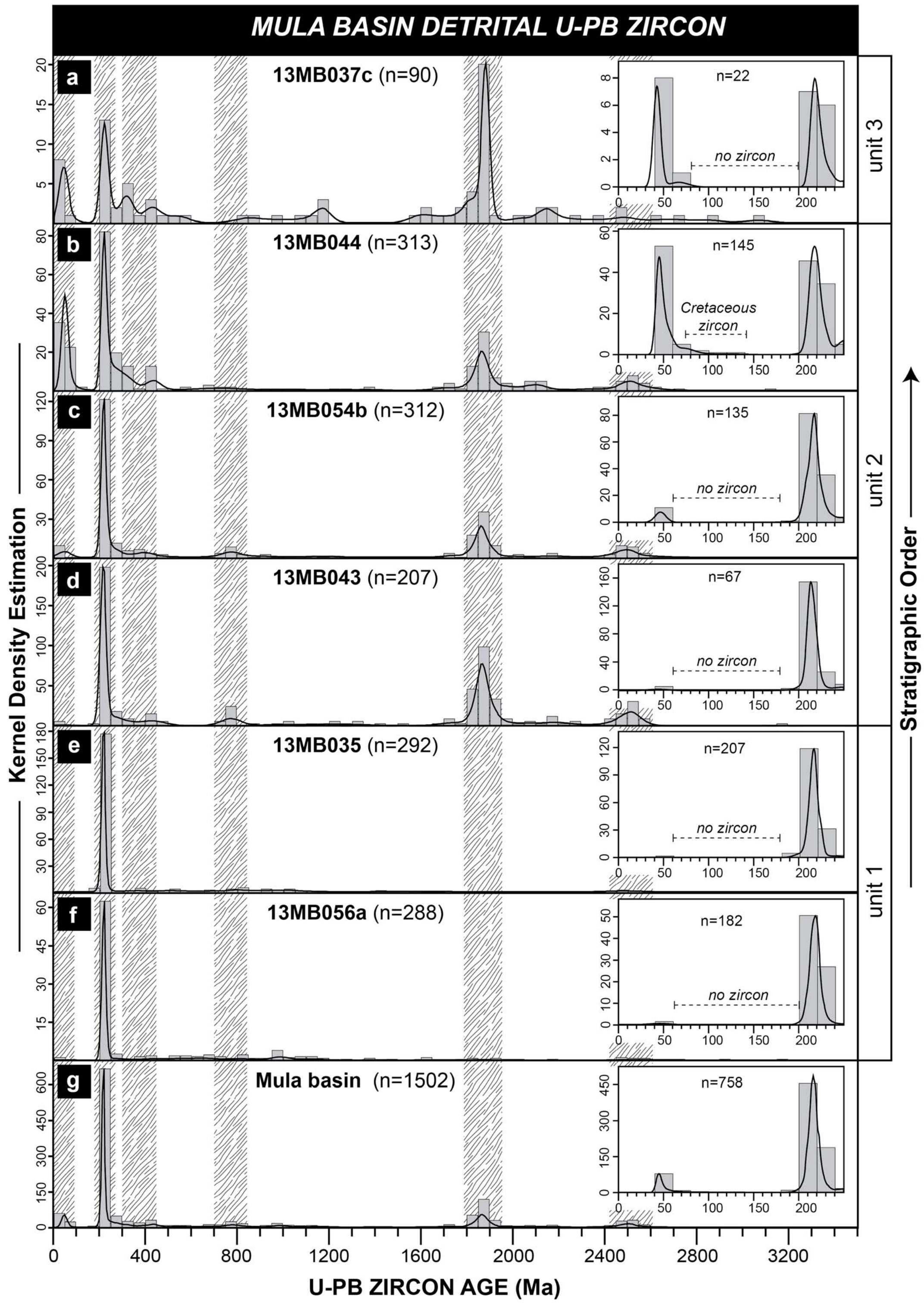

Figure 5. Detrital zircon geochronology results for the Mula basin. Each sample has been area corrected for plotting purposes. The black line represents a kernel density estimation calculated with a 15 bin size. The gray boxes represent 50-Ma histogram distribution of sample ages. Inserts represent 0–250 Ma for each corresponding sample.

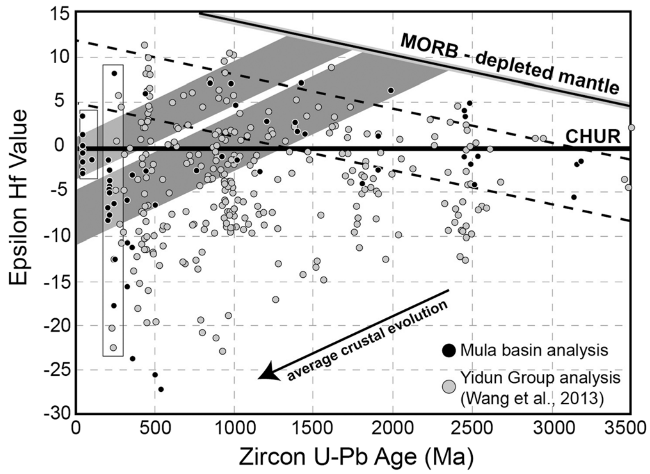

Figure 6. εHf data plotted with respect to U-Pb ages. Arrow illustrates path of Hf isotopic evolution of a typical felsic crust. The reference lines are as follows: MORB: depleted mantle; CHUR: chondritic uniform reservoir. The gray parallelograms show interpreted crustal evolution trajectories assuming present-day $^{176}Lu/^{177}Hf$.

6. Interpretations and Discussion

6.1. Depositional Environments

Clast compositions from conglomerate measurements are similar to the local bedrock of Triassic Daocheng Pluton and Yidun Group rock. We interpret the conglomerate layers in unit 1 to be deposited in an alluvial fan environment based on a predominately matrix-supported architecture, various clast size distribution and shapes, as well as the presence of have sheet bedding. Some conglomerate layers exhibit a clast-supported architecture, which presumably represents traction deposits associated with episodes of higher fluid flow (Gomez, 1991). Unit 2 deposits are interpreted to be streamflow alluvial fan environments. Planar cross-lamination in the sandstone intrabeds indicates current transport, and mudstone interbeds reflect either muddy debris-flows or pedogenic alteration of fine-grained streamflow alluvial deposits. The fine grained, planar-laminated siliciclastic deposits in unit 3 are interpreted to represent fine-grained streamflow alluvial facies. Overall, depositional environments suggest decreasing slope of the alluvial environment over time, either because of erosional degradation or subsidence along the basin margin, which would drive alluvial fan retrogradation and migration toward the hinterland (eastward).

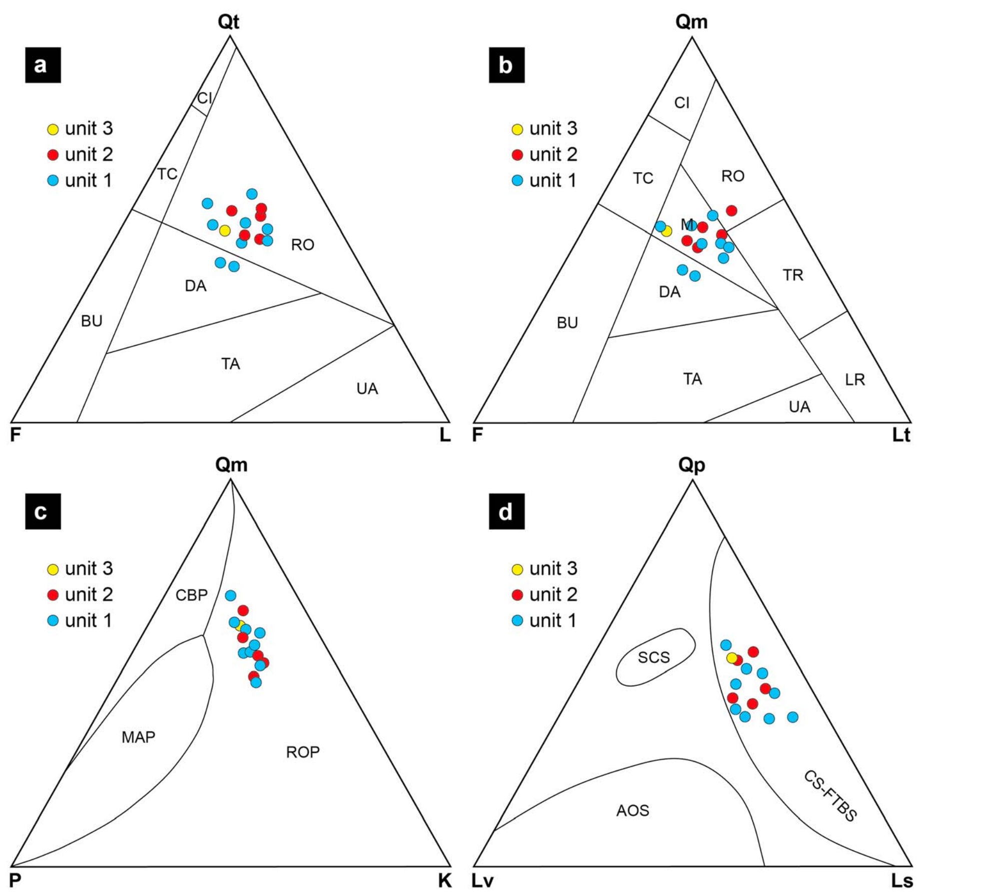

Figure 7. Petrology results from nine WGB and EGB samples. (a) Qt-F-L plot. CI: craton interior, TC: transitional continental, BU: basement uplift, RO: recycled orogenic, DA: dissected arc, TA: transitional arc, UA: undissected arc. (b) Qm-F-Lt plot. CI: craton interior, TC: transitional continental, BU: basement uplift, RO: recycled orogenic, M: mixed, DA: dissected arc, TA: transitional arc, TR: transitional recycled, LR: lithic recycled, UA: undissected arc. (c) Qm-P-K plot. CBP: continental block provenance, MAP: magmatic arc provenance, ROP: recycled orogen provenance. (d) Qp-Lv-Ls plot. SCS: subduction complex sources, AOS: arc orogen source, CS-FTBS: collision suture and fold-thrust belt sources.

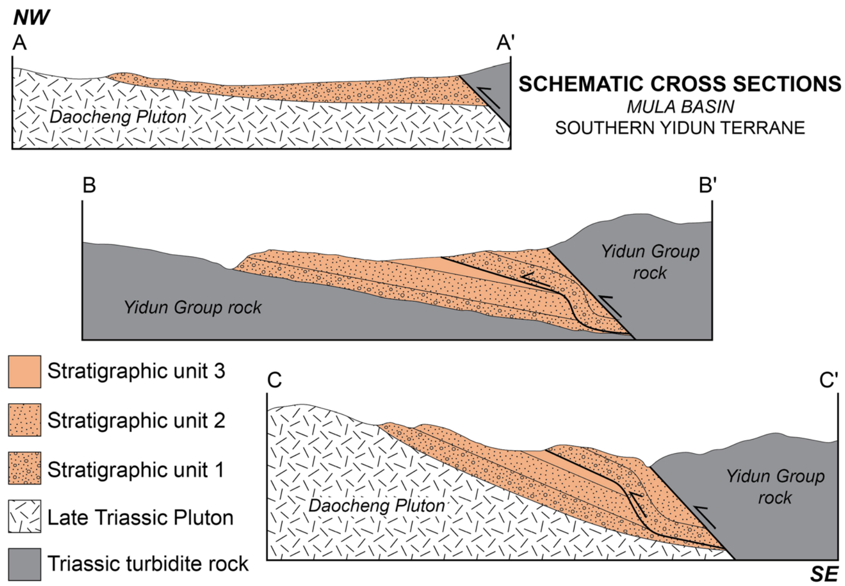

Figure 8. Schematic cross sections A-A′, B-B′, and C-C′ from the Mula basin. The cross-section line locations are shown in Figure 2b.

6.2. Age of Strata and Tectonic Setting

Assuming that surface uplift resulting from deformational phases correlates to cooling episodes, our geochronology results can be integrated with preexisting thermochronology in the eastern Tibetan Plateau to further evaluate the age of Mula basin strata. Investigations utilizing low-temperature thermochronology in the eastern Tibetan Plateau show Cenozoic cooling episodes in early Oligocene (29–33 Ma) and late Miocene (9–13 Ma) time (Arne et al., 1997; Kirby et al., 2002; Wang et al., 2012; Xu & Kamp, 2000). Investigations from the Daocheng Pluton, which the Mula basin overlies, record two Mesozoic cooling phases as well as the early Oligocene and early Miocene phases Early Cretaceous and early Miocene cooling episodes (Clark et al., 2005; Tian et al., 2014; Zhang et al., 2016).

Weighted mean averages for the youngest detrital zircon population from each sample yields Eocene age from ~43 to 47 Ma (Figure 9). When all Eocene grains are combined into a composite, the weighted mean average is 45.5 ± 0.5 Ma (Figure 9g), establishing an MDA for Mula basin strata. While there is no decreasing age trend upsection in our data, Eocene grains do become more prevalent in samples from the uppermost stratigraphic part of units 2 and 3. The lack of correlation between the stratigraphic position and the MDA for each sample suggests that the grains from the youngest detrital zircon population for each sample were shed from a source that predates nonmarine deposition. While our MDA of ~45 Ma precludes a Mesozoic age for the Mula basin, the possibility of either an Oligocene or Miocene age remains.

Field investigations in the eastern Tibetan Plateau show that Paleogene deformation consisted of contractional and some strike-slip features, associated with the northward impingement of the India plate to the southern margin of Eurasia (Tapponnier et al., 2001). During Oligocene time the dominant stress regime in the eastern Tibetan Plateau remained contractional; however, coeval strike-slip faulting in the region was established (Wang & Burchfiel, 1997). Since late Miocene time, strike-slip faulting has been the pervasive stress regime throughout the eastern Tibetan Plateau (Leloup et al., 1995; Zhang et al., 2015). The parallel trend relationship of the Mula basin thrust fault to the Triassic Ganzi-Litang suture precludes a tectonic setting interpretation associated with strike-slip deformation (i.e., restraining bend), which would promote oblique to perpendicular structural orientations between the suture and basin-bounding thrust fault. Therefore, based on structural indicators with regional stress regimes, our detrital zircon U-Pb geochronology results, and previously published thermochronology results, we prefer an interpretation of early Oligocene for the age of the Mula basin.

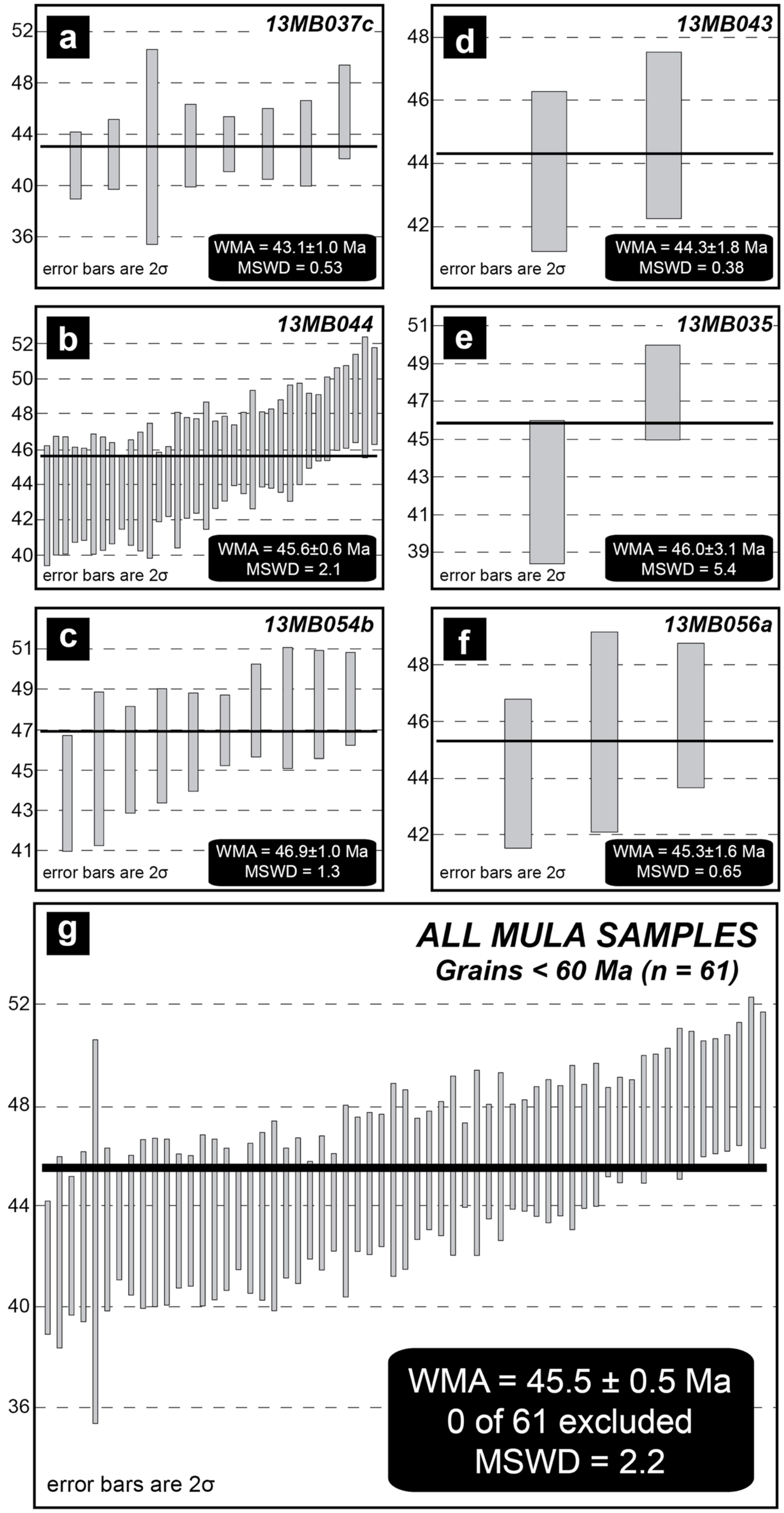

Figure 9. Weighted mean average plots illustrating maximum depositional ages for samples (a) 13MB037c, (b) 13MB044, (c) 13MB054b, (d) 13MB043, (e) 13MB035, (f) 13MB056a, and (g) a composite of all samples combined. The error bars represent 2σ error.

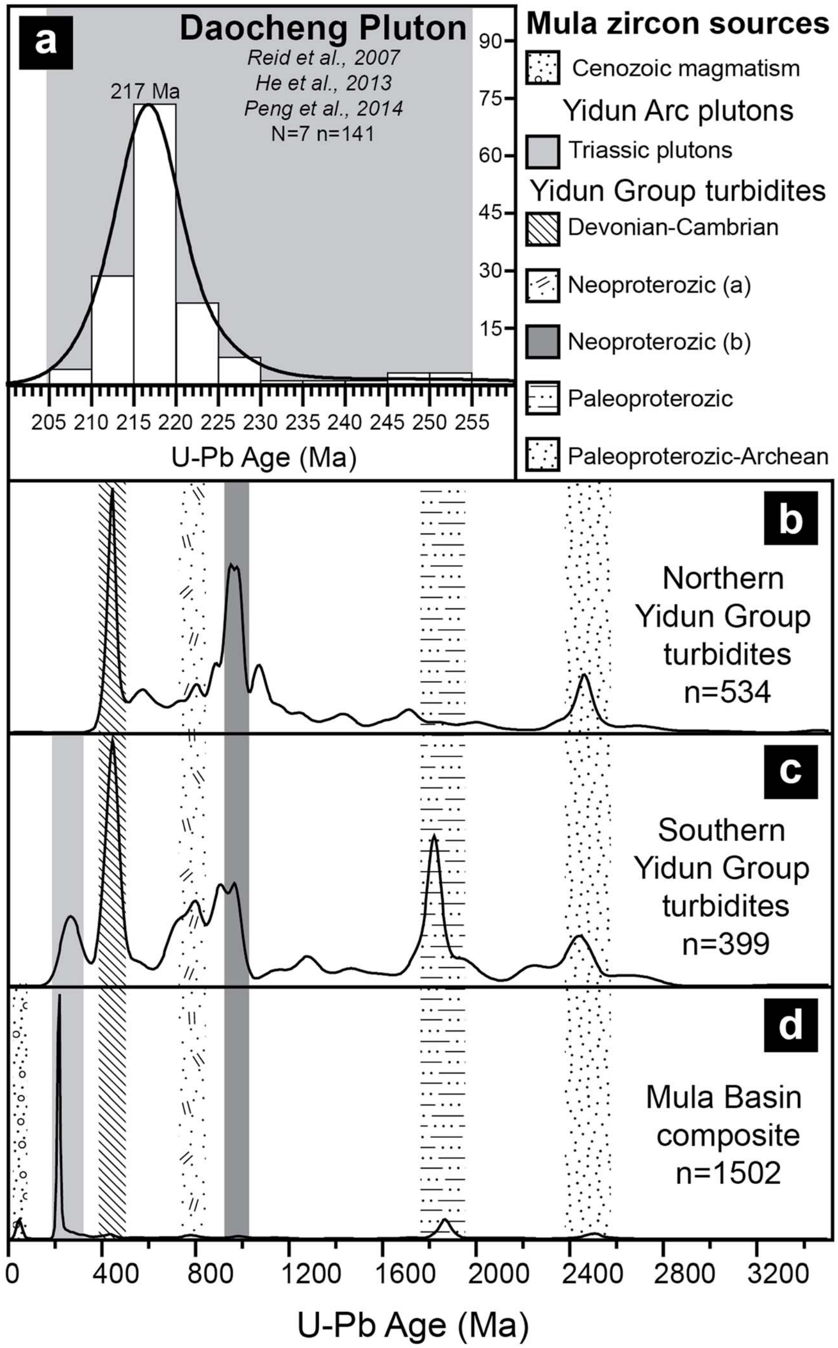

Figure 10. (a) U-Pb zircon results for the Triassic Daocheng pluton. (b and c) Regional detrital zircon geochronology results from the Triassic Yidun Group turbidites from Wang et al. (2013) and Ding et al. (2013). (d) Composite curve for Mula basin detrital zircon geochronology results. All age populations are represented by the combination of the Triassic Daocheng pluton (217 Ma) and Yidun Group turbidites.

6.3. Sedimentary Provenance

Field clast counts and thin section petrology suggest that Mula basin strata were sourced locally from the Triassic Daocheng Pluton and Triassic Yidun Group rocks. To identify the influence of these and other potential source rocks on the finer-grained basin fill, we compare the detrital zircon results to published zircon data sets for both the Daocheng Pluton and Yidun Group rocks (Figure 10). Compatibility is shown between Late Triassic zircon ages from the Daocheng Pluton and Triassic (215–225 Ma) detrital zircons from the Mula basin

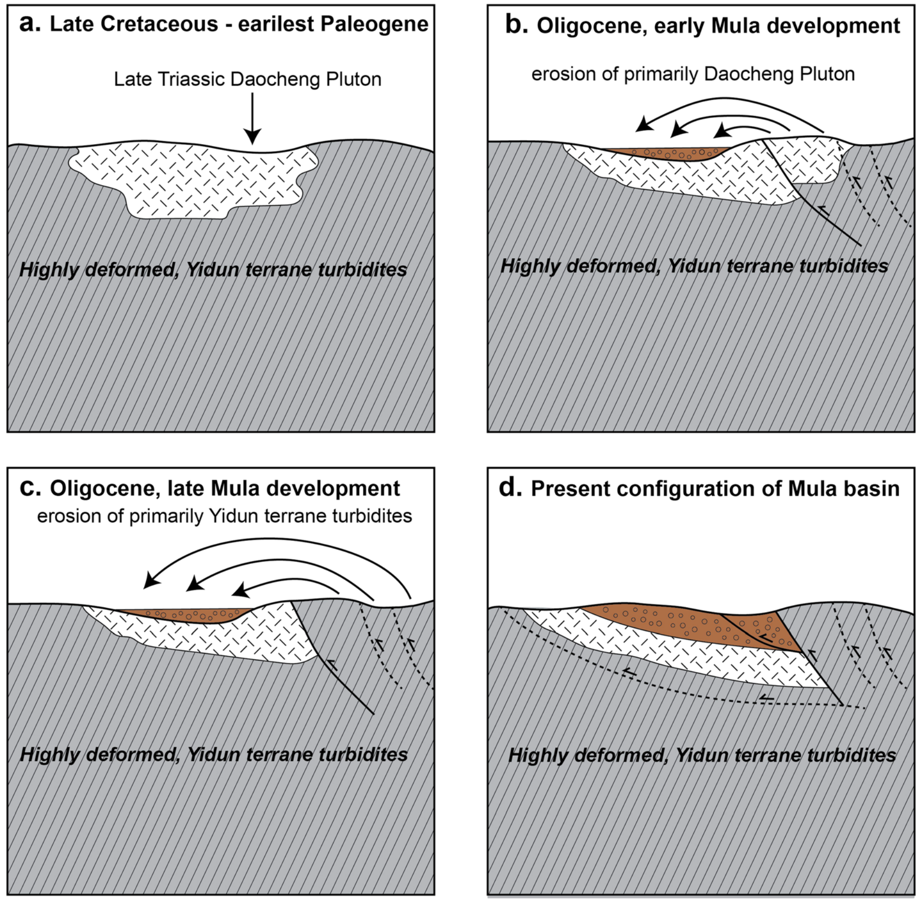

Figure 11. Animation summary of the early Cenozoic evolution of the Mula basin illustrating the progression of thin-skinned, thrust development and nonmarine basin fill, which resulted from uplift and erosion of Triassic Daocheng pluton and Yidun Group turbidite rock.

(Figure 10a). All other detrital age populations older than Late Triassic in the Mula strata are present in southern Yidun terrane turbidite detrital signatures (Figure 10b). Therefore, between the Daocheng Pluton and Yidun Group sources, all detrital zircon age populations in the Mula basin detrital zircon signature are accounted for except the Eocene population. We interpret these results to illustrate a local provenance for Mula basin strata.

Identifying the source for Eocene age grains remains puzzling. In other parts of the plateau, the emplacement of Eocene-Oligocene magmatic bodies is accompanied by the development of nonmarine basins, predominantly in close proximity to the Jinsha-Jiang and Bangong-Nujiang sutures (Chung et al., 2005; Q. Wang et al., 2008; C. Wang et al., 2008). Similar basin-pluton relationships also exist to the southeast around the Red River Shear Zone (Chung et al., 1998; LeLoup et al., 1995; Wang et al., 2001). Therefore, the likely source for the Eocene age population in Mula basin strata is a Cenozoic plutonic body in the eastern Tibetan Plateau (e.g., Roger et al., 2000). However, the nearest Cenozoic pluton (Haizi Pluton, Figure 2) is ~75 km to the west from the Mula basin, and paleoflow measurements indicate west-directed transport. The nearest Eocene pluton (Gongga Pluton) east of the Mula basin is presently located ~190 km to the east-northeast along the Xianshuihe fault (Arne et al., 1997; Xu & Kamp, 2000). Numerous Eocene plutons are present southeast of the Mula basin between the eastern Himalaya syntaxis and the Ailao Shan shear zone (Wang & Burchfiel, 1997), which upon paleorestoration would presumably have been more proximal to the basin during deposition. Other possible explanations for Eocene grains could include air transported grains.

The lack of Cretaceous grains in our detrital zircon data is interesting because of the proximity of the Cretaceous Haizi Pluton (Reid et al., 2007) to the Mula basin (e.g., Figure 2). The absence of Cretaceous

10.1029/2018TC004994

aged grains requires that either Cretaceous plutons were not exposed prior to the development of the Mula basin or that there was little extrusive magmatism associated with emplacement of these plutons, extrusive equivalents were removed by erosion prior to the timing of basin deposition, or that there was a negligible sediment contribution from the area that Cretaceous plutons currently occupy. Biotite Ar/Ar thermochronology shows that the Cretaceous plutons in the Yidun terrane passed through the blocking temperature at ~95 Ma, about 10 Myr after emplacement at ~105 Ma (Reid et al., 2007), presumably negating hypotheses that require Cretaceous plutons to remain unexposed. We interpret the lack to Cretaceous grains to be a consequence of geographic position at the time of Mula basin development because the Haizi Pluton is located to the west of the Mula basin and paleoflow measurements illustrate westward directed sediment transport.

Eocene and Triassic age εHf results from the Mula basin suggest the strata are sourced from Triassic Yidun Group and Triassic Yidun Arc rocks, which in turn were derived from Paleozoic and Neoproterozoic crust. εHf data from Yidun Group turbidites reveal magmatic reworking at ~2,000 and ~2,500 Ma, with the addition of juvenile material at 800–980 Ma, coinciding with episodic magmatism and crustal growth of the South China block (Yangtze) (Sun et al., 2009; Wang et al., 2010, 2013; Wang & Zhou, 2012). This correlation, along with an interpretation that the Zhongza Massif is of Yangtze block affinity (Chang, 2000; Song et al., 2004; Wang et al., 2013), would imply that Mula basin strata are primarily derived from recycling of the Yidun Group, which in turn was sourced from erosion of the Zhongza Massif.

The overwhelming amount of Late Triassic zircon grains suggest that the primary source for Mula sediment was the Daocheng Pluton, with older populations correlating to populations present in Triassic Yidun Group turbidites. A local sediment source is consistent with other studies of Paleogene nonmarine strata throughout the plateau (i.e., Horton et al., 2002; Spurlin et al., 2005; Studnicki-Gizbert et al., 2008), which show that in and north of the Qiangtang terrane, deposition was predominantly nonmarine and constricted to relatively small local drainage catchments.

6.4. Broader Implications

The tectonic development of the eastern Tibetan Plateau remains a central component to understanding the evolution of high topography and testing tectonic models. While studies indicate that the central plateau was at similar elevations as today in Eocene time (Hoke et al., 2014; Tang et al., 2017) and that the northern plateau experienced Eocene deformation and crustal thickening (Clark et al., 2010), uncertainties still remain pertaining to the eastern Tibetan Plateau. Since the onset of continent-continent collision between India-Asia, the eastern Tibetan Plateau has undergone multiple phases of deformation associated with the southeastern extrusion of crustal material. A thermochronology signature of slow Eocene cooling, followed by two rapid cooling episodes in early Oligocene and late Miocene time, presumably corresponds to the deformational episodes associated with crustal thickening (Zhang et al., 2016). This study illustrates that the Mula basin developed in a contractional tectonic setting (Figure 11), most likely in early Oligocene time, thereby bracketing the timing of and style of nonmarine deposition and deformation in the southern Yidun terrane. From a geodynamic perspective this allows for a better understanding of the timing of transition between contractional and strike-slip deformation in the eastern Tibetan Plateau.

7. Conclusions

Our investigation of the Mula basin, in the southern Yidun terrane, yields the following conclusions:

1. The Mula basin consists of ~1,000 m of nonmarine strata deposited in alluvial environments. Basin stratigraphic architecture can be separated into three units based primarily off of grain size that illustrates an overall fining upward trend.
2. The west boundary of the Mula basin is defined by unconformable contacts between nonmarine strata and the underlying Triassic Daocheng Pluton and Triassic Yidun Group rock. The Mula basin is bound to the east by a thrust fault that places Triassic Daocheng Pluton and Triassic Yidun Group rock on top of nonmarine strata. An intrabasin thrust fault, which exhibits a parallel trend to the basin-bounding fault, places older nonmarine strata on top of younger nonmarine strata in the southern part of the Mula basin. These structural and stratigraphic relationships indicate that the Mula basin developed in a contractional tectonic regime and that deformation occurred after deposition of nonmarine strata.
3. A maximum depositional age of 45.5 ± 0.5 Ma, calculated from the youngest detrital zircon population (s), brackets an Eocene or younger age for the Mula basin. Combined with structural observations and

previously reported thermochronology results, an Oligocene age for the development of the Mula basin is proposed.

4. Field clast counts, thin section petrology, detrital zircon geochronology, and εHf isotope results show that the Mula basin strata were primarily sourced from local, relatively small, drainage systems consisting of Triassic Daocheng Pluton and Triassic Yidun Group rocks.
5. The Mula basin developed as a far-field, upper-crustal response associated with the plateau outgrowth resulting from the India-Asia collision, prior to the onset of dominant strike-slip deformation throughout the eastern Tibetan Plateau.

Acknowledgments
This work was supported by the U.S. National Science Foundation grants EAR-1119266 (Robinson) and EAR-1119219 (Weislogel). The University of Alabama Graduate School and Department of Geological Sciences provided travel support. Chunmiao Zheng (Peking University) provided assistance with field permits. Zircon U-Pb and εHf analyses were conducted at the University of Arizona's LaserChron Center. Fei Shang assisted in the field and provided many constructive discussions on the regional tectonic development. We thank Sam Hansen, Alison Duvall, Rezene Mahatsente, and Matt Wielicki for reading versions of this manuscript for Jackson's dissertation. Thorough reviews by Huiping Zhang, Paul Kapp, and an anonymous reviewer greatly improved the manuscript. All data are provided in the present manuscript and Tables S1 (field measurements), S2 (detrital U-Pb zircon geochronology), S3 (εHf isotope analyses), and S4 (thin section petrology).

References

Arne, D., Worley, B., Wilson, C., Chen, S. F., Foster, D., Luo, Z. L., et al. (1997). Differential exhumation in response to episodic thrusting along the eastern margin of the Tibetan Plateau. *Tectonophysics*, *280*(3-4), 239–256. https://doi.org/10.1016/S0040-1951 (97)00040-1

Barbeau, D. L. Jr., Gombosi, D. J., Zahid, K. M., Bizimis, M., Swanson-Hysell, N., Valencia, V., & Gehrels, G. (2009). U-Pb zircon constraints on the age and provenance of the Rocas Verdes basin fill, Tierra del Fuego, Argentina. *Geochemistry, Geophysics, Geosystems*, *10*, Q12001. https://doi.org/10.1029/2009GC002749

Black, L. P., Kamo, S. L., Allen, C. M., Davis, D. W., Aleinikoff, J. N., Valley, J. W., et al. (2004). Improved 206Pb/238U microprobe geochronology by the monitoring of a trace-element-related matrix effect; SHRIMP, ID-TIMS, ELA-ICP-MS and oxygen isotope documentation for a series of zircon standards. *Chemical Geology*, *205*(1-2), 115–140. https://doi.org/10.1016/j.chemgeo. 2004.01.003

Burchfiel, B. C., Chen, Z., Liu, Y., & Royden, L. H. (1995). Tectonics of the Longmen Shan and adjacent regions. *International Geology Review*, *37*(8), 661–735. https://doi.org/10.1080/00206819509465424

Burchfiel, B. C., & Chen, Z. L. (2012). Tectonics of the southeastern Tibetan Plateau and its adjacent Foreland. *Geological Society of America Memior*, *210*, 231.

Bureau of Geology and Mineral Resources of Sichuan Province (1991). Regional geology of Sichuan Province. Geological memoirs of PRC Ministry of Geology and Mineral Resources. In *In Chinese with English Summary* (p. 730). Geological Publishing House, Beijing.

Carrapa, B., bin Hassim, M. F., Kapp, P. A., DeCelles, P. G., & Gehrels, G. (2017). Tectonic and erosional history of southern Tibet recorded by detrital chronological signatures along the Yarlung River drainage. *Geological Society of America Bulletin*, *129*(5-6), 570–581. https://doi.org/10.1130/B31587.1

Chang, E. Z. (2000). Geology and tectonics of the Songpan-Ganzi fold belt, southwestern China. *International Geology Review*, *42*(9), 813–831. https://doi.org/10.1080/00206810009465113

Chung, S. L., Chu, M. F., Zhang, Y., Xie, Y., Lo, C. H., Lee, T. Y., et al. (2005). Tibetan tectonic evolution inferred from spatial and temporal variations in post-collisional magmatism. *Earth Science Reviews*, *68*(3-4), 173–196. https://doi.org/10.1016/j.earscirev. 2004.05.001

Chung, S. L., Lo, C. H., Lee, T. Y., Zhang, Y. Q., Xie, Y. W., Li, X. H., et al. (1998). Diachronous uplift of the Tibetan Plateau starting 40 Myr ago. *Nature*, *394*(6695), 769–773. https://doi.org/10.1038/29511

Clark, M. K., Bush, J. W. M., & Royden, L. H. (2005). Dynamic topography produced by lower crustal flow against rheological strength heterogeneities bordering the Tibetan Plateau. *Geophysical Journal International*, *162*(2), 575–590. https://doi.org/10.1111/j.1365-246X.2005.02580.x

Clark, M. K., Farley, K. A., Zheng, D., Wang, Z., & Duvall, A. R. (2010). Early Cenozoic faulting of the northern Tibetan Plateau margin from apatite (U-Th)/He ages. *Earth and Planetary Science Letters*, *296*(1–2), 78–88. https://doi.org/10.1016/j.epsl.2010.04.051

Clark, M. K., & Royden, L. H. (2000). Topographic ooze: Building the eastern margin of Tibet by lower crustal flow. *Geology*, *28*, 703–706. https://doi.org/10.1130/0091-7613(2000)28<703:TOBTEM>2.0.CO;2

Craddock, W. H., Kirby, E., Dewen, Z., & Jianhui, C. (2012). Tectonic setting of Cretaceous basins on the NE Tibetan Plateau: Insights from the Jungong basin. *Basin Research*, *24*(1), 51–69. https://doi.org/10.1111/j.1365-2117.2011.00515.x

Currie, B. S., Polissar, P. J., Rowley, D. B., Ingalls, M., Li, S., Olack, G., & Freeman, K. H. (2016). Multiproxy paleoaltimetry of the late Oligocene-Pliocene Oiyug Basin, southern Tibet. *American Journal of Science*, *316*(5), 401–436. https://doi.org/10.2475/05.2016.01

Dai, J., Zhao, X., Wang, C., Zhu, L., Li, Y., & Finn, D. (2012). The vast proto-Tibetan Plateau: New constraints from Paleogene Hoh Xil Basin. *Gondwana Research*, *22*(2), 434–446. https://doi.org/10.1016/j.gr. 2011.08.019

Dayem, K. E., Molnar, P., Clark, M. K., & Houseman, G. A. (2009). Far-field lithospheric deformation in Tibet during continental collision. *Tectonics*, *28*, TC6005. https://doi.org/10.1029/2008TC002344

DeCelles, P. G., Carrapa, B., & Gehrels, G. E. (2007). Detrital zircon U-Pb ages provide new provenance and chronostratigraphic information from Eocene synorogenic deposits in northwestern Argentina. *Geology*, *35*(4), 323–326. https://doi.org/10.1130/G23322A.1

DeCelles, P. G., Kapp, P., Ding, L., & Gehrels, G. E. (2007). Late Cretaceous to middle Tertiary basin evolution in the central Tibetan Plateau: Changing environments in response to tectonic partitioning, aridification, and regional elevation gain. *Geological Society of America Bulletin*, *119*(5-6), 654–680. https://doi.org/10.1130/B26074.1

DeCelles, P. G., Kapp, P., Gehrels, G. E., & Ding, L. (2014). Paleocene-Eocene foreland basin evolution in the Himalaya of southern Tibet and Nepal: Implications for the age of initial India-Asia collision. *Tectonics*, *33*, 824–849. https://doi.org/10.1002/2014TC003522

DeCelles, P. G., Robinson, D. M., & Zandt, G. (2002). Implications of shortening in the Himalayan fold-thrust belt for uplift of the Tibetan Plateau. *Tectonics*, *21*(6), 1062. https://doi.org/10.1029/2001TC001322

Dehler, C. M., Fanning, C. M., Link, P. K., Kingsbury, E. M., & Rybczynski, D. (2010). Maximum depositional age and provenance of the Uinta Mountain Group and Big Cottonwood Formation, northern Utah: Paleogeography of rifting western Laurentia. *Geological Society of America Bulletin*, *122*(9-10), 1686–1699. https://doi.org/10.1130/B30094.1

Dewey, J., Shackleton, R., Chang, C. F., & Sun, Y. Y. (1988). The tectonic evolution of the Tibetan Plateau. *Philosophical Transactions of the Royal Society of London*, *327*(1594), 379–413. https://doi.org/10.1098/rsta.1988.0135

Dickinson, W. R. (1970). Interpreting detrital modes of greywacke and arkose. *Journal of Sedimentary Petrology*, *40*, 695–707.

Dickinson, W. R. (1985). Interpreting provenance relations from detrital modes of sandstones. In G. G. Zuffa (Ed.), *Provenance of arenites* (pp. 333–361). Boston: D. Reidel Publishing.

Dickinson, W. R., & Gehrels, G. E. (2003). U-Pb ages of detrital zircons from Permian and Jurassic eolian sandstones of the Colorado Plateau, USA; paleogeographic implications. *Sedimentary Geology*, *163*(1-2), 29–66. https://doi.org/10.1016/S0037-0738(03)00158-1

Dickinson, W. R., & Gehrels, G. E. (2009). Use of U-Pb ages of detrital zircons to infer maximum depositional ages of strata: A test against a Colorado Plateau Mesozoic database. *Earth and Planetary Science Letters*, *288*(1-2), 115–125. https://doi.org/10.1016/j.epsl. 2009.09.013

Dickinson, W. R., & Suczek, C. (1979). Plate tectonics and sandstone compositions. *American Association of Petroleum Geologists Bulletin*, *63*, 2164–2182.

Ding, L., Kapp, P., & Wan, X. (2005). Paleocene-Eocene record of ophiolite obduction and initial India-Asia collision, south central Tibet. *Tectonics*, *24*, TC3001. https://doi.org/10.1029/2004TC001729

Ding, L., Xu, Q., Yue, Y., Wang, H., Cai, F., & Li, S. (2014). The Andean-type Gangdese Mountains: Paleoelevation record from the Paleocene-Eocene Linzhou Basin. *Earth and Planetary Science Letters*, *392*, 250–264. https://doi.org/10.1016/j.epsl. 2014.01.045

Ding, L., Yang, D., Cai, F. L., Pullen, A., Kapp, P., Gehrels, G. E., et al. (2013). Provenance analysis of the Mesozoic Hoh-Xil-Songpan-Ganzi turbidites in Northern Tibet: Implications for the tectonic evolution of the eastern Paleo-Tethys Ocean. *Tectonics*, *32*, 34–48. https://doi.org/10.1002/tect. 20013

England, P., & Houseman, G. (1986). Finite strain calculations of continental deformation: Comparison with the India-Asia collision zone. *Journal of Geophysical Research*, *91*, 3664–3676. https://doi.org/10.1029/JB091iB03p03664

England, P., & Houseman, G. (1989). Extension during continental convergence, with application to the Tibetan Plateau. *Journal of Geophysical Research*, *94*, 17,561–17,579. https://doi.org/10.1029/JB094iB12p17561

England, P., & McKenzie, D. (1982). A thin viscous sheet model for continental deformation. *Geophysical Journal International*, *70*(2), 295–321. https://doi.org/10.1111/j.1365-246X.1982.tb04969.x

England, P., & Searle, M. (1986). The Cretaceous-Tertiary deformation of the Lhasa Block and its implications for crustal thickening in Tibet. *Tectonics*, *5*, 1–14. https://doi.org/10.1029/TC005i001p00001

Fildani, A., Cope, T. D., Graham, S. A., & Wooden, J. L. (2003). Initiation of the Magallanes foreland basin: Timing of the southernmost Patagonian Andes orogeny revised by detrital zircon provenance analysis. *Geology*, *31*(12), 1081–1084. https://doi.org/10.1130/G20016.1

Gehrels, G., & Pecha, M. (2014). Detrital zircon U-Pb geochronology and Hf isotope geochemistry of Paleozoic and Triassic passive margin strata of western North America. *Geosphere*, *10*(1), 49–65. https://doi.org/10.1130/GES00889.1

Gehrels, G., Valencia, V., & Pullen, A. (2006). Detrital zircon geochronology by laser-ablation multicollector ICPMS at the Arizona LaserChron Center, in, Geochronology: Emerging Opportunities Pap. 12, T. Loszewski and W. Huff (eds.). *Paleontological Society Papers*, *12*, 67–76.

Gehrels, G. E. (2014). Detrital zircon U-Pb geochronology applied to tectonics. *Annual Review of Earth and Planetary Sciences*, *42*(1), 127–149. https://doi.org/10.1146/annurev-earth-050212-124012

Gehrels, G. E., Valencia, V., & Ruiz, J. (2008). Enhanced precision, accuracy, effiency, and spatial resolution of U-Pb ages by laser ablation-multicollector-inductively coupled plasma-mass spectrometry. *Geochemistry, Geophysics, Geosystems*, *9*, Q03017. https://doi.org/10.1029/2007GC001805

Gomez, B. (1991). Bedload transport. *Earth Science Reviews*, *31*(2), 89–132. https://doi.org/10.1016/0012-8252(91)90017-A

Haihong, C., Dobson, J., Heller, F., & Jie, H. (1995). Paleomagnetic evidence for clockwise rotation of the Simao region since Cretaceous: A consequence of India-Asia collision. *Earth and Planetary Science Letters*, *134*(1-2), 203–217. https://doi.org/10.1016/0012-821X (95)00118-V

He, D. F., Zhu, W. G., Zhong, H., Ren, T., Bai, Z. J., & Fan, H. P. (2013). Zircon U-Pb geochronology and elemental and Sr-Nd-Hf isotopic geochemistry of the Daocheng granitic pluton from the Yidun Arc, SW China. *Journal of Asian Earth Science*, *67-68*, 1–17. https://doi.org/10.1016/j.jseaes.2013.02.002

Hoke, G. D., Liu-Zeng, J., Hren, M. T., Wissink, G. K., & Garzione, C. N. (2014). Stable isotopes reveal high southeast Tibetan Plateau margin since the Paleogene. *Earth and Planetary Science Letters*, *394*, 270–278. https://doi.org/10.1016/j.epsl.2014.03.0070012-821X/

Holt, W. E., Ni, J. F., Wallace, T. C., & Haines, A. J. (1991). The active tectonics of the eastern Himalayan syntaxis and surrounding regions. *Journal of Geophysical Research*, *96*, 14,595–14,632. https://doi.org/10.1029/91JB01021

Horton, B. K., Dupont-Nivet, G., Zhou, J., Waanders, G. L., Butler, R. F., & Wang, J. (2004). Mesozoic-Cenozoic evolution of the Xining-Minhe and Dangchang basins, northeastern Tibetan Plateau: Magnetostratigraphic and biostratigraphic results. *Journal of Geophysical Research*, *109*, B04402. https://doi.org/10.1029/2003JB002913

Horton, B. K., Yin, A., Spurlin, M. S., Zhou, J., & Wang, J. (2002). Paleocene-Eocene syncontractional sedimentation in narrow, lacustrine-dominated basins of east-central Tibet. *Geological Society of America Bulletin*, *114*, 771–786. https://doi.org/10.1130/0016-7606(2002)114<0771

Hou, Z. (1993). Tectonic-magmatic evolution of the Yidun island-arc and geodynamic setting of kuroko-type sulfide deposits in Sanjiang The Region, SW China. In S. Ishihara, T. Urabe, & H. Ohmoto (Eds.), *Mineral resources symposia; volume C. Selected papers from the symposia I-3-47, II-16-5, II-16-10 and II-16-12, ferro-manganese deposits, anoxic sediments and massive sulfide deposits*, *Shigen Chishitsu Special Issue* (Vol. 17, pp. 336–350). Japan: Society of Resource Geologists of Japan, Tokyo.

Hou, Z., Mo, X., Tan, J., Hu, S., & Luo, Z. (1993). The eruption sequences of basalts in the Yidun island arc, Sanjiang region and evolution of rift to island arc. *Bulletin of China Academy of Geological Science*, *26*, 4–67.

Hu, X., Garzanti, E., Wang, J., Huang, W., An, W., & Webb, A. (2016). The timing of India-Asia collision onset—Facts, theories, controversies. *Earth-Science Reviews*, *160*, 264–299. https://doi.org/10.1016/j.earscirev.2016.07.014

Huang, K., & Opdyke, N. (1993). Paleomagnetic results from Cretaceous and Jurassic rocks from Southwest Yunnan: Evidence for large clockwise rotations in the Indochina and Shan-Thai-Malay terranes. *Earth and Planetary Science Letters*, *117*(3-4), 507–524. https://doi.org/10.1016/0012-821X(93)90100-N

Ingalls, M., Rowley, D., Olack, G., Currie, B., Li, S., Schmidt, J., et al. (2018). Paleocene to Pliocene low-latitude, high-elevation basins of southern Tibet: Implications for tectonic models of India-Asia collision, Cenozoic climate, and geochemical weathering. *Geological Society of America Bulletin*, *130*(1-2), 307–330. https://doi.org/10.1130/B31723.1

Ingersoll, R. V. (1978). Petrofacies and petrologic evolution of the Late Cretaceous forearc basin, northern and central California. *The Journal of Geology*, *86*(3), 335–352. https://doi.org/10.1086/649695

Ingersoll, R. V., Bullard, T. F., Ford, R. L., Grimm, J. P., Pickle, J. D., & Sares, S. W. (1984). The effect of grain size on detrital modes: A test of the Gazzi-Dickinson point-counting method. *Journal of Sedimentary Petrology*, *54*(1), 103–116. https://doi.org/10.1306/212F83B9-2B24-11D7-8648000102C1865D

Kapp, P., DeCelles, P. G., Gehrels, G. E., Heizler, M., & Ding, L. (2007). Geological records of the Lhasa-Qiangtang and Indo-Asian collisions in the Nima area of central Tibet. *Geological Society of America Bulletin*, *119*(7-8), 917–933. https://doi.org/10.1130/B26033.1

Kapp, P., Yin, A., Harrison, T. M., & Ding, L. (2005). Cretaceous-Tertiary shortening, basin development, and volcanism in central Tibet. *Geological Society of America Bulletin*, *117*(7), 865–878. https://doi.org/10.1130/B25595.1

Kapp, P., Yin, A., Manning, C. E., Harrison, T. M., Taylor, M. H., & Ding, L. (2003). Tectonic evolution of the early Mesozoic blueschist-bearing Qiangtang metamorphic belt, central Tibet. *Tectonics*, *22*(4), 1043. https://doi.org/10.1029/2002TC001383

Kirby, E., Reiners, P. W., Krol, M. A., Whipple, K. X., Hodges, K. V., Farley, K. A., et al. (2002). Late Cenozoic evolution of the eastern margin of the Tibetan Plateau: Inferences from 40Ar/39Ar and (U-Th)/He thermochronology. *Tectonics*, *21*(1), 1001. https://doi.org/10.1029/2000TC001246

Kroner, A., Greiling, R., Reischmann, T., Hussein, I. R. M., Stern, R. J., Durr, S., et al. (1987). Pan-African crustal evolution in the Nubian segment of Northeast Africa. In A. Kroner (Ed.), *Proterozoic lithosphere evolution*, *American Geophysical Union Geodynamics Series* (Vol. 17, pp. 235–257). https://doi.org/10.1029/GD017p0235

Leary, R., Orme, D. A., Laskowski, A. K., DeCelles, P. G., Kapp, P., Carrapa, B., & Dettinger, M. (2016). Along-strike diachroneity in the deposition of the Kailas Formation in central southern Tibet: Implications for Indian slab dynamics. *Geosphere*, *12*(4), 1198–1223. https://doi.org/10.1130/GESO1325.1

Leary, R. J., DeCelles, P. G., Quade, J., Gehrels, G. E., & Waanders, G. (2016). The Liuqu conglomerate, southern Tibet: Early Miocene basin development related to deformation within the Great Counter Thrust system. *Lithosphere*, *8*(5), 427–450. https://doi.org/10.1130/L542.1

Leech, M. L., Singh, S., Jain, A. K., Klemperer, S. L., & Manickavasagam, R. M. (2005). The onset of India-Asia continental collision: Early, steep subduction required by the timing of UHP metamorphism in the western Himalaya. *Earth and Planetary Science Letters*, *234*(1–2), 83–97. https://doi.org/10.1016/j.epsl. 2005.02.038

Leier, A. L., DeCelles, P. G., Kapp, P., & Ding, L. (2007). The Takena Formation of the Lhasa terrane, southern Tibet: The record of a Late Cretaceous retroarc foreland basin. *Geological Society of America Bulletin*, *119*(1-2), 31–48. https://doi.org/10.1130/B25974.1

Leier, A. L., Kapp, P., Gehrels, G. E., & DeCelles, P. G. (2007). Detrital zircon geochronology of Carboniferous-Cretaceous strata in the Lhasa terrane, southern Tibet. *Basin Research*, *19*(3), 361–378. https://doi.org/10.1111/j.1365-2117.2007.00330.x

LeLoup, P. H., Lacassin, R., Tapponnier, P., Scharer, U., Zhong, D., Liu, X., et al. (1995). The Ailao Shan-Red River shear zone (Yunnan, China), Tertiary transform boundary of Indochina. *Tectonophysics*, *251*(1-4), 13–84. https://doi.org/10.1016/0040-1951(95)00070-4

Li, S., Currie, B. S., Rowley, D. B., & Ingalls, M. (2015). Cenozoic paleoaltinetry of the SE margin of the Tibetan Plateau: Constraints on the tectonic evolution of the region. *Earth and Planetary Science Letters*, *432*, 415–424. https://doi.org/10.1016/j.epsl.2015.09.0440012-821X/

Lippert, P. C., van Hinsbergen, D. J. J., & Dupont-Nivet, G. (2014). Early Cretaceous to present latitude of the central proto-Tibetan Plateau: A paleomagnetic synthesis with implications for Cenozoic tectonics, paleogeography, and climate of Asia. *Geological Society of America Special Papers*, *507*, 1–21. https://doi.org/10.1130/2014.2507(01)

Liu, Z., & Wang, C. (2001). Facies analysis and depositional systems of Cenozoic sediments in the Hoh Xil basin, northern Tibet. *Sedimentary Geology*, *140*(3-4), 251–270. https://doi.org/10.1016/S0037-0738(00)00188-3

Liu, Z., Wang, C., & Yi, H. (2001). Evolution and mass accumulations of the Cenozoic Hoh Xil basin, northern Tibet. *Journal of Sedimentary Research*, *71*(6), 971–984. https://doi.org/10.1306/030901710971

Liu, Z., Zhao, X., Wang, C., Liu, S., & Yi, H. (2003). Magnetostratigraphy of Tertiary sediments from the Hoh Xil Basin: Implications for the Cenozoic tectonic history of the Tibetan Plateau. *Geophysical Journal International*, *154*(2), 233–252. https://doi.org/10.1046/j.1365-246X.2003.01986.x

Ludwig, K. R. (2012). A geochronological toolkit for Microsoft Excel. *Berkeley Geochronology Center Special Publication*, *5*, 75.

Meade, B. J. (2007). Present-day kinematics at the India-Asia collision zone. *Geology*, *35*(1), 81–84. https://doi.org/10.1130/G22924A.1

Molnar, P., England, P., & Martinod, J. (1993). Mantle dynamics, uplift of the Tibetan Plateau, and the Indian monsoon. *Reviews in Geophysics*, *31*, 357–396. https://doi.org/10.1029/93RG02030

Murphy, M. A., Yin, A., Harrison, T. M., Durr, S. B., Chen, Z., Ryerson, F. J., et al. (1997). Did the Indo-Asian collision along create the Tibetan Plateau? *Geology*, *25*(8), 719–722. https://doi.org/10.1130/0091-7613(1997)025<0719:DTIACA>2.3.CO;2

Nabelek, J., Hetenyi, G., Vergne, J., Sapkota, S., Kafle, B., Jiang, M., et al. (2009). Underplating in the Himalaya-Tibet collision zone revealed by the Hi-CLIMB experiment. *Science*, *325*(5946), 1371–1374. https://doi.org/10.1126/science. 1167719

Najman, Y., Appel, E., Boudagher-Fadel, M., Bown, P., Carter, A., Garzanti, E., et al. (2010). Timing of the India-Asia collision: Geological, biostratigraphic, and paleomagnetic constraints. *Journal of Geophysical Research*, *115*, B12416. https://doi.org/10.1029/2010JB007673

Nelson, D. R. (2001). An assessment of the determination of depositional ages for Precambrian clastic sedimentary rocks by U-Pb dating of detrital zircon. *Sedimentary Geology*, *141-142*, 37–60. https://doi.org/10.1016/S0037-0738(01)00067-7

Orme, D. A., Carrapa, B., & Kapp, P. (2015). Sedimentology, provenance and geochronology of the upper Cretaceous-lower Eocene western Xigaze forearc basin, southern Tibet. *Basin Research*, *27*(4), 387–411. https://doi.org/10.1111/bre.12080

Owens, T. J., & Zandt, G. (1997). Implications of crustal property variations for models of Tibetan Pateau evolution. *Nature*, *387*(6628), 37–43. https://doi.org/10.1038/387037a0

Peng, T., Zhao, G., Fan, W., Peng, B., & Mao, Y. (2014). Zircon geochronology and Hf isotopes of Mesozoic intrusive rocks from the Yidun terrane, Eastern Tibetan Plateau: Petrogenesis and their bearings with Cu mineralization. *Journal of Asian Earth Sciences*, *80*, 18–33. https://doi.org/10.1016/j.jseaes.2013.10.028

Powell, C. M. A. (1986). Continental underplating model for the rise of the Tibetan Plateau. *Earth and Planetary Science Letters*, *81*(1), 79–94. https://doi.org/10.1016/0012-821X(86)90102-0

Pullen, A., Kapp, P., Gehrels, G. E., DeCelles, P. G., Brown, E., Fabijanic, J. M., & Ding, L. (2008). Gandese retroarc thrust belt and foreland basin deposits in the Damxung area, southern Tibet. *Journal of Asian Earth Sciences*, *33*(5-6), 323–336. https://doi.org/10.1016/j.jseaes. 2008.01.005

Pullen, A., Kapp, P., Gehrels, G. E., Vervoort, J. D., & Ding, L. (2008). Triassic continental subduction in central Tibet and Mediterranean-style closure of the Paleo-Tethys Ocean. *Geology*, *36*(5), 351–354. https://doi.org/10.1130/G24435A.1

Reid, A. J., Wilson, C. J. L., & Liu, S. (2005). Structural evidence for the Permo-Triassic tectonic evolution of the Yidun arc, eastern Tibetan Plateau. *Journal of Structural Geology*, *27*(1), 119–137. https://doi.org/10.1016/j.jsg. 2004.06.011

Reid, A. J., Wilson, C. J. L., Liu, S., Pearson, N., & Belousova, E. (2007). Mesozoic plutons of the Yidun arc, SW China: U/Pb geochronology and Hf isotopic signature. *Ore Geology Reviews*, *31*(1-4), 88–106. https://doi.org/10.1016/j.oregeorev. 2004.11.003

Roger, F., Jolivet, M., & Malavieille, J. (2010). The tectonic evolution of the Songpan-Garze (North Tibet) and adjacent areas from Proterozoic to present: A synthesis. *Journal of Asian Earth Sciences*, *39*(4), 254–269. https://doi.org/10.1016/j.jseaes. 2010.03.008

Roger, F., Tapponnier, P., Arnaud, N., Scharer, U., Brunel, M., Zhiqin, X., & Jingsui, Y. (2000). An Eocene magmatic belt across central Tibet: Mantle subduction triggered by the Indian collision? *Terra Nova*, *12*(3), 102–108. https://doi.org/10.1046/j.1365-3121.2000.123282.x

Rowley, D. B., & Currie, B. S. (2006). Palaeo-altimetry of the late Eocene to Miocene Lunpola basin, central Tibet. *Nature*, *439*(7077), 677–681. https://doi.org/10.1038/nature04506

Royden, L. H., Burchfiel, B. C., King, R. W., Wang, E., Chen, Z., Shen, F., & Liu, Y. (1997). Surface deformation and lower crustal flow in eastern Tibet. *Science*, *276*(5313), 788–790. https://doi.org/10.1126/science. 1155371

Royden, L. H., Burchfiel, B. C., & van der Hilst, R. D. (2008). The geological evolution of the Tibetan Plateau. *Science*, *321*(5892), 1054–1058. https://doi.org/10.1126/science.1155371

Schoenbohm, L. M., Burchfiel, B. C., Chen, L., & Yin, J. (2005). Exhumation of the Ailao Shan shear zone recorded by Cenozoic sedimentary rocks, Yunnan Province, China. *Tectonics*, *24*, TC6015. https://doi.org/10.1029/2005TC001803

Schoenbohm, L. M., Burchfiel, B. C., & Liangzhong, C. (2006). Propagation of surface uplift, lower crustal flow, and Cenozoic tectonics of the southeast margin of the Tibetan Plateau. *Geology*, *34*(10), 813–816. https://doi.org/10.1130/G22679.1

Sircombe, K. N. (1999). Tracing provenance through the isotope ages of littoral and sedimentary detrital zircon, eastern Australia. *Sedimentary Geology*, *124*(1-4), 47–67. https://doi.org/10.1016/S0037-0738(98)00120-1

Song, X. Y., Zhou, M. F., Cao, Z. M., & Robinson, P. T. (2004). Late Permian rifting of the South China Craton caused by the Emeishan mantle plume? *Journal of the Geological Society, London*, *161*(5), 773–781. https://doi.org/10.1144/0016-764903-135

Spurlin, M. S., Yin, A., Horton, B. K., Zhou, J., & Wang, J. (2005). Structural evolution of the Yushu-Nangqian region and its relationship to syn-collisional igneous activity, east-central Tibet. *Geological Society of America Bulletin*, *117*(9), 1293–1317. https://doi.org/10.1130/B25572.1

Staisch, L. M., Niemi, N. A., Hong, C., Clark, M. K., Rowley, D. B., & Currie, B. (2014). A Cretaceous-Eocene depositional age for the Fenghuoshan Group, Hoh Xil Basin: Implications for the tectonic evolution of the northern Tibet Plateau. *Tectonics*, *33*, 281–301. https://doi.org/10.1002/2013TC003367

Studnicki-Gizbert, C., Burchfiel, B. C., Li, Z., & Chen, Z. (2008). Early Tertiary Gonjo basin, eastern Tibet: Sedimentary and structural record of the early history of India-Asia collision. *Geosphere*, *4*(4), 713–735. https://doi.org/10.1130/GES00136.1

Sun, W., Zhou, M., Gao, J., Yang, Y., Zhao, X., & Zhao, J. (2009). Detrital zircon U-Pb geochronological and Lu-Hf isotopic constraints on the Precambrian magmatic and crustal evolution of the western Yangtze block, SW China. *Precambrian Research*, *172*(1-2), 99–126. https://doi.org/10.1016/j.precamres. 2009.03.010

Surpless, K. D., Graham, S. A., Covault, J. A., & Wooden, J. L. (2006). Does the Great Valley Group contain Jurassic strata? Reevaluation of the age and early evolution of a classic forearc basin. *Geology*, *34*(1), 21–24. https://doi.org/10.1130/G21940.1

Tang, M., Liu-Zeng, J., Hoke, G. D., Xu, Q., Wang, W., Li, Z., et al. (2017). Paleoelevation reconstruction of the Paleocene-Eocene Gonjo basin, SE-central Tibet. *Tectonophysics*, *712-713*, 170–181. https://doi.org/10.1016/j.tecto.2017.05.018

Tapponnier, P., Peltzer, G., Le Dain, A. Y., Armijo, R., & Cobbold, P. (1982). Propagating extrusion tectonics in Asia: New insights from simple experiments with plasticine. *Geology*, *10*, 611–616. https://doi.org/10.1130/0091-7613(1982)10<611:PETIAN>2.0.CO;2

Tapponnier, P., Zhiqin, X., Roger, F., Meyer, B., Arnaud, N., Wittlinger, G., & Jingsui, Y. (2001). Oblique stepwise rise and growth of the Tibet Plateau. *Science*, *294*(5547), 1671–1677. https://doi.org/10.1126/science. 105978

Thatcher, W. (2007). Microplate model for the present-day deformation of Tibet. *Journal of Geophysical Research*, *112*, B01401. https://doi.org/10.1029/2005JB004244

Tian, Y., Kohn, B. P., Gleadow, A. J. W., & Hu, S. (2014). A thermochronological perspective on the morphotectonic evolution of the south-eastern Tibetan Plateau. *Journal of Geophysical Research: Solid Earth*, *119*, 676–698. https://doi.org/10.1002/2013JB010429

Van der Voo, R., Spakman, W., & Bijwaard, H. (1999). Tethyan subducted slabs under India. *Earth and Planetary Science Letters*, *171*, 7–20.

Vermeesch, P. (2004). How many grains are needed for a provenance study? *Earth and Planetary Science Letters*, *224*(3-4), 441–451. https://doi.org/10.1016/j.epsl. 2004.05.037

Vermeesch, P. (2012). On the visualization of detrital age distributions. *Chemical Geology*, *312–313*, 190–194. https://doi.org/10.1016/j.chemgeo. 2012.04.021

Wang, B. Q., Wang, W., Chen, W. T., Gao, J. F., Zhao, X. F., Yan, D. P., & Zhou, M. F. (2013). Constraints of detrital zircon U-Pb ages and Hf isotopes on the provenance of the Triassic Yidun Group and tectonic evolution of the Yidun Terrane, eastern Tibet. *Sedimentary Geology*, *289*, 74–98. https://doi.org/10.1016/j.sedgeo.2013.02.005

Wang, C., Zhao, X., Liu, Z., Lippert, P. C., Graham, S. A., Coe, R. S., et al. (2008). Constraints on the early uplift history of the Tibetan Plateau. *Proceedings from the National Academy of Sciences*, *105*(13), 4987–4992. https://doi.org/10.1073/pnas.0703595105

Wang, E., & Burchfiel, B. C. (1997). Interpretation of Cenozoic tectonics in the right-lateral accommodation zone between the Ailao Shan shear zone and the eastern Himalayan syntaxis. *International Geology Review*, *39*(3), 191–219. https://doi.org/10.1080/00206819709465267

Wang, E., & Burchfiel, B. C. (2000). Late Cenozoic to Holocene deformation in southwest Sichuan and adjacent Yunnan, China, and its role in formation of the southeastern part of the Tibetan Plateau. *Geological Society of America Bulletin*, *112*, 413–423. https://doi.org/10.1130/0016-7606(2000)112<413:LCTHDI>2.0.CO;2

Wang, E., Kirby, E., Furlong, K. P., van Soest, M., Xu, G., Shi, X., et al. (2012). Two-phase growth of high topography in eastern Tibet during the Cenozoic. *Nature Geoscience*, *5*, 640–645. https://doi.org/10.1038/ngeo1538

Wang, J., Hu, X., Jansa, L., & Huang, Z. (2011). Provenance of the Upper Cretaceous-Eocene deep-water sandstones in Sangdanlin, southern Tibet: Constraints on the timing of initial India-Asia collision. *The Journal of Geology*, *119*(3), 293–309. https://doi.org/10.1086/659145

Wang, J. H., Yin, A., Harrison, T. M., Grove, M., Zhang, Y. Q., & Xie, G. H. (2001). A tectonic model for Cenozoic igneous activities in the eastern Indo-Asian collision zone. *Earth and Planetary Science Letters*, *188*(1-2), 123–133. https://doi.org/10.1016/S0012-821X(01)00315-6

Wang, L., Pan, G., Li, D., Xu, Q., & Lin, S. (1999). The spatio-temporal framework and geological evolution of the Jinshajiang arc-basin systems. *Acta Geologica Sinica*, *73*, 206–218. (in Chinese)

Wang, Q., Wyman, D. A., Xu, J., Dong, Y., Vasconcelos, P. M., Pearson, N., et al. (2008). Eocene melting of subducting continental crust and early uplifting of central Tibet: Evidence from central-western Qiangtang high-K calc-alkaline andesites, dacites and rhyolites. *Earth and Planetary Science Letters*, *272*(1–2), 158–171. https://doi.org/10.1016/j.epsl. 2008.04.034

Wang, S., Fang, X., Zheng, D., & Wang, E. (2009). Initiation of slip along the Xianshuihe fault zone, eastern Tibet, constrained by K/Ar and fission-track ages. *International Geology Review*, *51*(12), 1121–1131. https://doi.org/10.1080/00206810902945132

Wang, W., Wang, F., Chen, F., Zhu, X., Xiao, P., & Siebel, W. (2010). Detrital zircon ages and Hf–Nd isotopic composition of Neoproterozoic sedimentary rocks in the Yangtze block: Constraints on the deposition age and provenance. *The Journal of Geology*, *118*(1), 79–94. https://doi.org/10.1086/648533

Wang, W., & Zhou, M. F. (2012). Sedimentary records of the Yangtze block (South China) and their correlation with equivalent Neoproterozoic sequences on adjacent continents. *Sedimentary Geology*, *265–266*, 126–142. https://doi.org/10.1016/j.sedgeo 012.04.003

Xu, G., & Kamp, P. J. J. (2000). Tectonics and denudation adjacent to the Xianshuihe fault, eastern Tibetan Plateau: Constraints from fission track thermochronology. *Journal of Geophysical Research*, *105*, 19,231–19,251. https://doi.org/10.1029/2000JB900159

Xu, Q., Ding, L., Hetzel, R., Yue, Y., & Rades, E. F. (2015). Low elevation of the northern Lhasa terrrane in the Eocene: Implications for relief development in South Tibet. *Terra Nova*, *27*(6), 458–466. https://doi.org/10.1111/ter.12180

Yin, A., & Harrison, T. M. (2000). Geologic evolution of the Himalayan-Tibetan orogeny. *Annual Reviews of Earth Planet Science*, *28*(1), 211–280. https://doi.org/10.1146/annurev.earth.28.1.211

Yin, J., Xu, J., Liu, C., & Li, H. (1988). The Tibetan Plateau: Regional stratigraphic context and previous work. *Philosophical Transactions of the Royal Society of London*, *327*, 5–52.

Zahid, K. M., & Barbeau, D. L. Jr. (2011). Constructing sandstone provenance and classification ternary diagrams using an electronic spreadsheet. *Journal of Sedimentary Research*, *81*(9), 702–707. https://doi.org/10.2110/jsr.2011.55

Zhang, H., Oskin, M. E., Liu-Zeng, J., Zhang, P., Reiners, P. W., & Xiao, P. (2016). Pulsed exhumation of interior eastern Tibet: Implications for relief generation mechanisms and the origin of high-elevation planation surfaces. *Earth and Planetary Science Letters*, *449*, 176–185. https://doi.org/10.1016/j.epsl.2016.05.048

Zhang, K., Zhang, Y., Tang, X., & Xia, B. (2012). Late Mesozoic tectonic evolution and growth of the Tibetan Plateau prior to the Indo-Asian collision. *Earth-Science Reviews*, *114*(3–4), 236–249. https://doi.org/10.1016/j.earscirev. 2012.06.001

Zhang, N., Cao, Y., Lio, Y. A., Zhao, Y., Zhang, H., Hu, D., et al. (1998). *Geology and metallogeny in the Garze-Litang rift zone*. Beijing: Geological Publishing House.

Zhang, Y., & Zheng, J. (1994). *Geological survey of the Hoh Xil and adjacent regions in Qinghai Province* (p. 177). Beijing: Seismological Press.

Zhang, Y. Z., Replumaz, A., Wang, G. C., Leloup, P. H., Gautheron, C., Bernet, M., et al. (2015). Timing and rate of exhumation along the Litang fault system, implication for fault reorganization in Southeast Tibet. *Tectonics*, *34*, 1219–1243. https://doi.org/10.1002/2014TC003671

Zhang, Z. M., Zhao, G. C., Santosh, M., Wang, J. L., Dong, X., & Liou, J. G. (2010). Two stages of granulite facies metamorphism in the eastern Himalayan syntaxis, South Tibet: Petrology, zircon geochronology and implications for the subduction of Neo-Tethys and the Indian continent beneath Asia. *Journal of Metamorphic Geology*, *28*, 719–733. https://doi.org/10.1111/j.1525-1314.2010.00885.x

Zhao, W. L., & Morgan, W. J. (1987). Injection of Indian crust into Tibetan lower crust: A two-dimensional finite element model study. *Tectonics*, *6*, 489–504. https://doi.org/10.1029/TC006i004p00489